AD-A127 432 DESIGN STUDY OF A TOROIDAL ELECTROSTATIC ANALYZER(U) 1/2
AIR FORCE INST OF TECH WRIGHT-PATTERSON AFB OH SCHOOL
OF ENGINEERING R L HARTLEY DEC 82 AFIT/GEP/PH/82D-11
UNCLASSIFIED F/G 14/2 NL

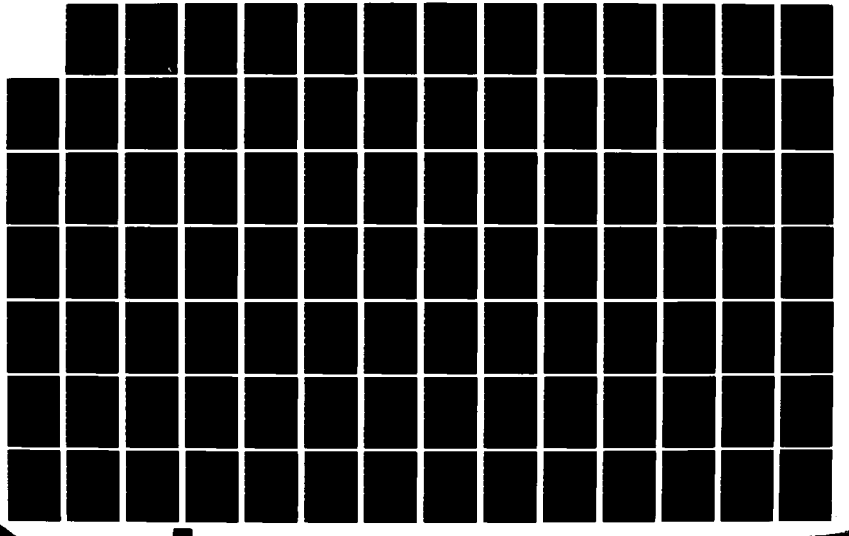

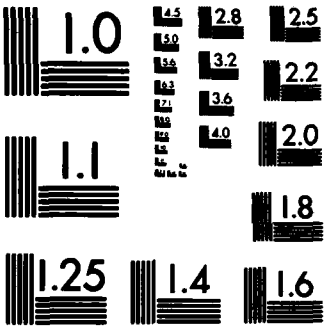

MICROCOPY RESOLUTION TEST CHART
NATIONAL BUREAU OF STANDARDS-1963-A

DESIGN STUDY OF A TOROIDAL ELECTROSTATIC ANALYZER

THESIS

AFIT/GEP/PH/82D-11 Robert L. Hartley, Jr.
Capt USAF

DEPARTMENT OF THE AIR FORCE
AIR UNIVERSITY (ATC)
AIR FORCE INSTITUTE OF TECHNOLOGY

Wright-Patterson Air Force Base, Ohio

AFIT/GEP/PH/82D-11

DESIGN STUDY OF A TOROIDAL ELECTROSTATIC ANALYZER

THESIS

AFIT/GEP/PH/82D-11 Robert L. Hartley, Jr.
Capt USAF

AFIT/GEP/PH/82D-11

DESIGN STUDY

OF A

TOROIDAL ELECTROSTATIC ANALYZER

THESIS

Presented to the faculty of the School of Engineering

of the Air Force Institute of Technology

Air University

in Partial Fulfillment of the

Requirements for the Degree of

Master of Science

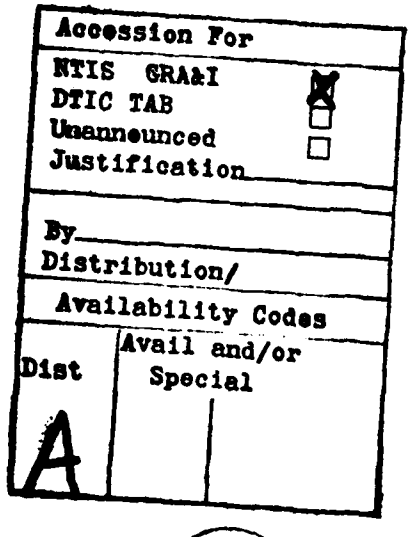

by

Robert L. Hartley, Jr., B.S.

Capt USAF

Graduate Engineering Physics

December 1982

Approved for public release; distribution unlimited

Preface

This thesis is a preliminary design study of a toroidal electrostatic analyzer with multiple, off-center slits. The use of off-center slits provides one with multiple data channels, with each channel sampling at a different energy. Thus, energy spectra can be obtained in a fraction of the time normally required by an analyzer with a single entrance-exit slit pair.

I would like to thank my thesis advisor, Major James Lange, for his encouragement and frequent help which was so essential for the completion of my thesis. I am also grateful to 1Lt John Glessner and 1Lt Glenn Param, whose conversations were of frequent aid.

Finally, I wish to give my special thanks to my wife, Carol, for her patience and assistance throughout my thesis. If not for her loving support, this paper might never have reached its completion.

Robert LaVerne Hartley, Jr.

Contents

Contents

List of Figures

List of Figures

List of Symbols

r,ϕ,z	cylindrical coordinates
r_a,r_b	radial, radii of inner/outer electrodes
R_a,R_b	axial, radii of inner/outer electrodes
a_e,R_e	radial/axial radii of mid-electrode surface
ϕ_e	angular extent of electrodes
$\rho \equiv \frac{r-a_e}{a_e}$	dimensionless, radial coordinate
$\zeta \equiv \frac{z}{a_e}$	dimensionless, axial coordinate
ρ_0,ζ_0	radial/axial coordinates of a point in entry slit
ρ_1,ζ_1	radial/axial coordinates of a point at field boundary
β_1,β_2,β_3	constants in electric field series solution
$U(\rho,\zeta)$	electric potential
U_0	± voltage on electrodes
E_r,E_ϕ,E_z	electric field components
E_0	central path, radial electric field strength
M_0	specific ion mass
γ	parameter, much less than one
$M=M_0(1+\gamma)$	mass of any ion
v_0	specific ion velocity
β	parameter, much less than one
$v'=v_0(1+\beta)$	ion velocity outside of field
v	ion velocity inside of field
e	ion unit charge

List of Symbols

$eE_0 = \frac{-M_0 v_0^2}{a_e}$	centripetal force equation, defines M_0, v_0, E_0
$\varepsilon^2 \equiv \frac{a_e}{R_e}$	ratio of radii, math constant
$\chi^2 = \lvert 2 - \frac{a_e}{R_e} \rvert$	geometrical, math constant
$\delta = \frac{\gamma+2}{\chi^2}$	math constant
$T_0 = \frac{1}{2} M_0 v_0^2$	specific kinetic energy
T	kinetic energy of ion outside of field
$\eta = \frac{T-T_0}{T_0}$	relative energy of an ion
α_r', α_z'	radial/axial entry angles
α_r'', α_z''	radial/axial exit angles
x', y', z'	entrance coordinate system
x'', y'', z''	exit coordinate system
ℓ'	object plane location, primary entrance slit location
ℓ_r'', ℓ_z''	radial/axial image plane location, exit slit location
g_r, g_z	radial/axial focal point locations
f_r, f_z	radial/axial "Focal lengths"
G_r, G_z	radial/axial magnifications
R_{rel}	relative energy resolution
R_{abs}	absolute energy resolution
$T(\eta)$	transmission
w', w''	entry/exit slit widths
$K \ (w' = Ka_e)$	entry slit width parameter

Abstract

The design of a toroidal, electrostatic analyzer is discussed with special emphasis on the instrument providing multiple channels of data by sampling different points of the energy spectra simultaneously. Two additional results of this study are that a toroidal analyzer can have four times the resolution of a spherical analyzer and can cover sixteen times as much of the energy spectra (with a fixed electrode voltage).

The electrostatics, equations of motion, and the optic equations are discussed. The applications chapter discusses the use of multiple, off-center slits, the minimization of the size of the instrument, the trade-offs that must be made in designing an instrument, the effect of field errors, the minimization of the effects of the field errors, and the total beam current as seen by the detector. Included in the Appendix are design curves that should be of assistance to the reader in designing his own instrument.

I. Introduction

A. Background

Electrostatic analyzers are used to measure the charge to energy ratio of ions. Their function can perhaps best be explained with a simple example. Let an ion of mass, M, and charge, q, enter a pair of parallel plates (see Figure 1) with energy, $T_0 = \frac{1}{2} MV_x^2$. We will assume that the electric field is purely in the y-direction and that the initial conditions are $x(o) = 0$, $\dot{X}(o) = V_x$, $y(o) = 0$, $\dot{y}(o) = 0$. The equation of motion is given by

$$M\ddot{y} = qEy \tag{1-1}$$

with solution

$$y(t) = \frac{qEy}{2M} t^2 \tag{1-2}$$

The ion travels through the electrodes in a time, $t_1 = L/V_x$. We may now write equation (1-2) as

$$y(t_1) = \left(\frac{EyL^2}{4}\right)\left(\frac{q}{T_0}\right) \tag{1-3}$$

Equation (1-3) shows us that the ion's position, as it exits the electrodes, is a direct measure of the ion's charge to energy ratio.

Traditionally, an electrostatic analyzer has fixed entrance and exit slits attached to it. Only those ions with a specific charge to energy ratio will be transmitted. A detector behind the exit slit provides a count of the number of ions with this specific charge to

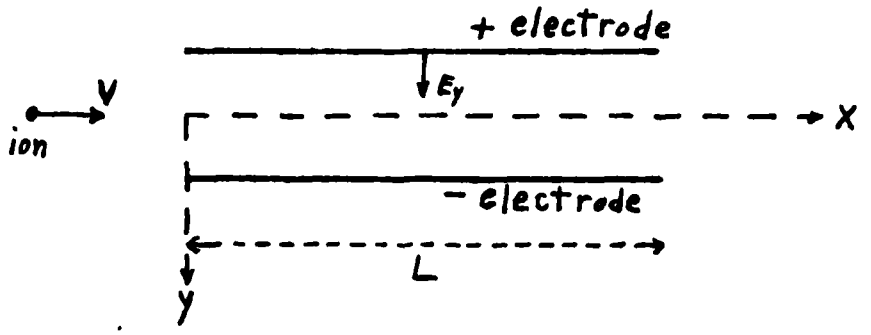

ion mass $\equiv M$

ion charge $\equiv q$

electrode

length $\equiv L$

initial

energy, $T_o \equiv \frac{1}{2} M V_x^2$

initial conditions

$X(0) = 0$

$\dot{X}(0) = V_x$

$y(0) = 0$

$\dot{y}(0) = 0$

ignore fringe fields

Figure 1 - Parallel Plate Example - Side View

energy ratio. By varying the voltage applied to the electrodes, a complete q/T_0 spectra can be obtained. Furthermore, if q is known, then the energy spectra can be measured directly. In this paper the charge will be folded into the centripetal force and will not show explicitly as q/T_0. The energy will be given by itself without reference to the charge.

The four most common types of electrostatic analyzers have parallel plate electrodes, concentric cylindrical electrodes, concentric spherical electrodes, and toroidal electrodes. The toroidal electrode surfaces are described by two distinct radii, r and R, with different centers (see Figure 2). The toroidal electrodes are more general in that they contain the cylindrical electrodes, $R = \infty$, and the spherical electrodes, $R = r$, as special cases.

The parallel plate analyzer is restricted in its resolution due to the limited angle through which it can deflect the beam. The cylindrical, spherical, and toroidal analyzers all have better resolution than the parallel plate analyzer. Because of their rotational symmetry, they can deflect the ion beam through a larger angle, thus achieving better energy dispersion. However, the cylindrical analyzer has no axial focusing, thus the beam spreads out axially, which lowers the beam intensity. Due to their double curvature, both the spherical and toroidal analyzers have axial focusing, which helps to maintain the beam intensity. Since the cylindrical and spherical analyzers are both special cases of the toroidal analyzer, only the toroidal analyzer will be developed in this paper. When

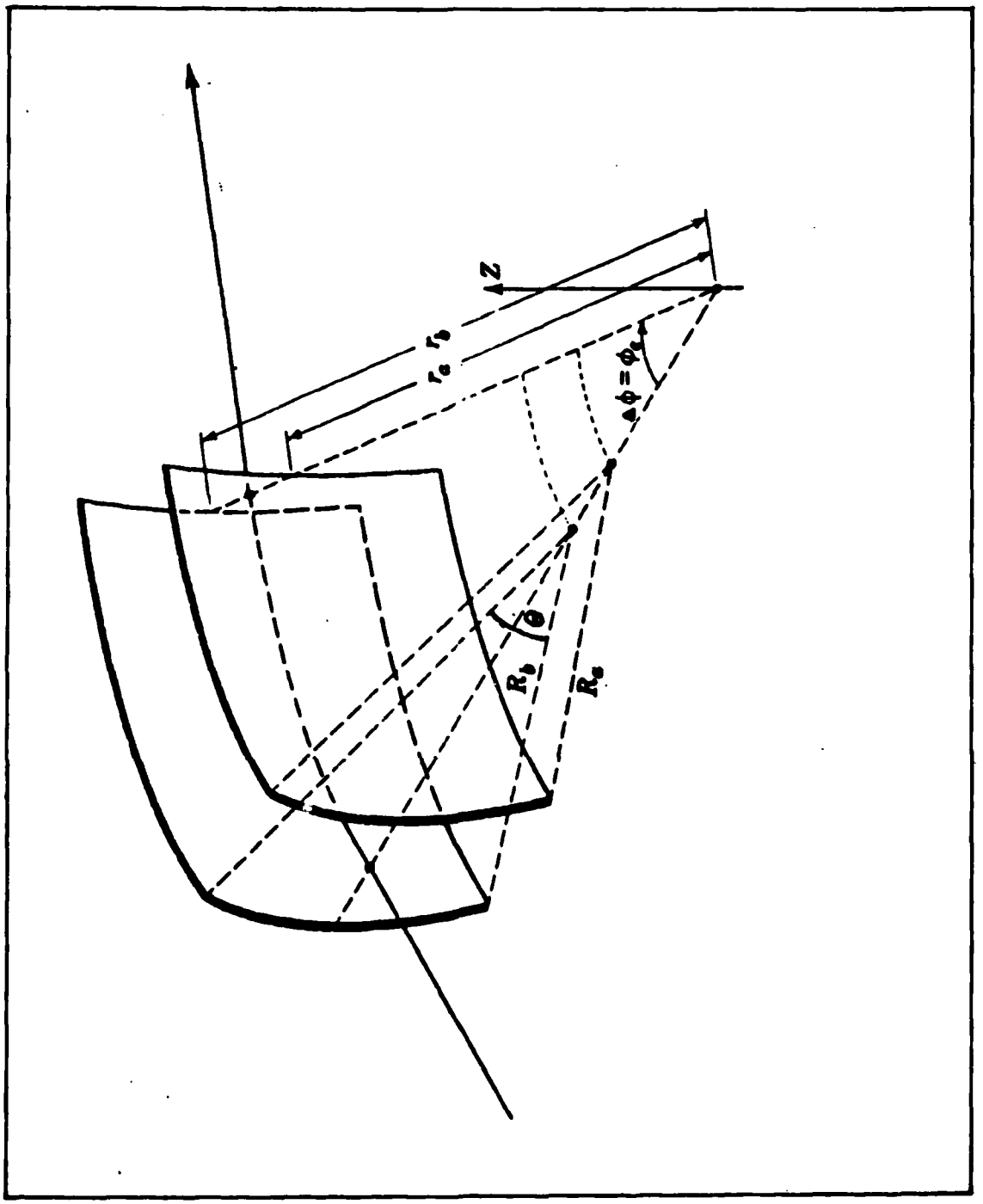

Figure 2 - Cylindrical Coordinate System
(From Ewald and Liebl, ref. 2)

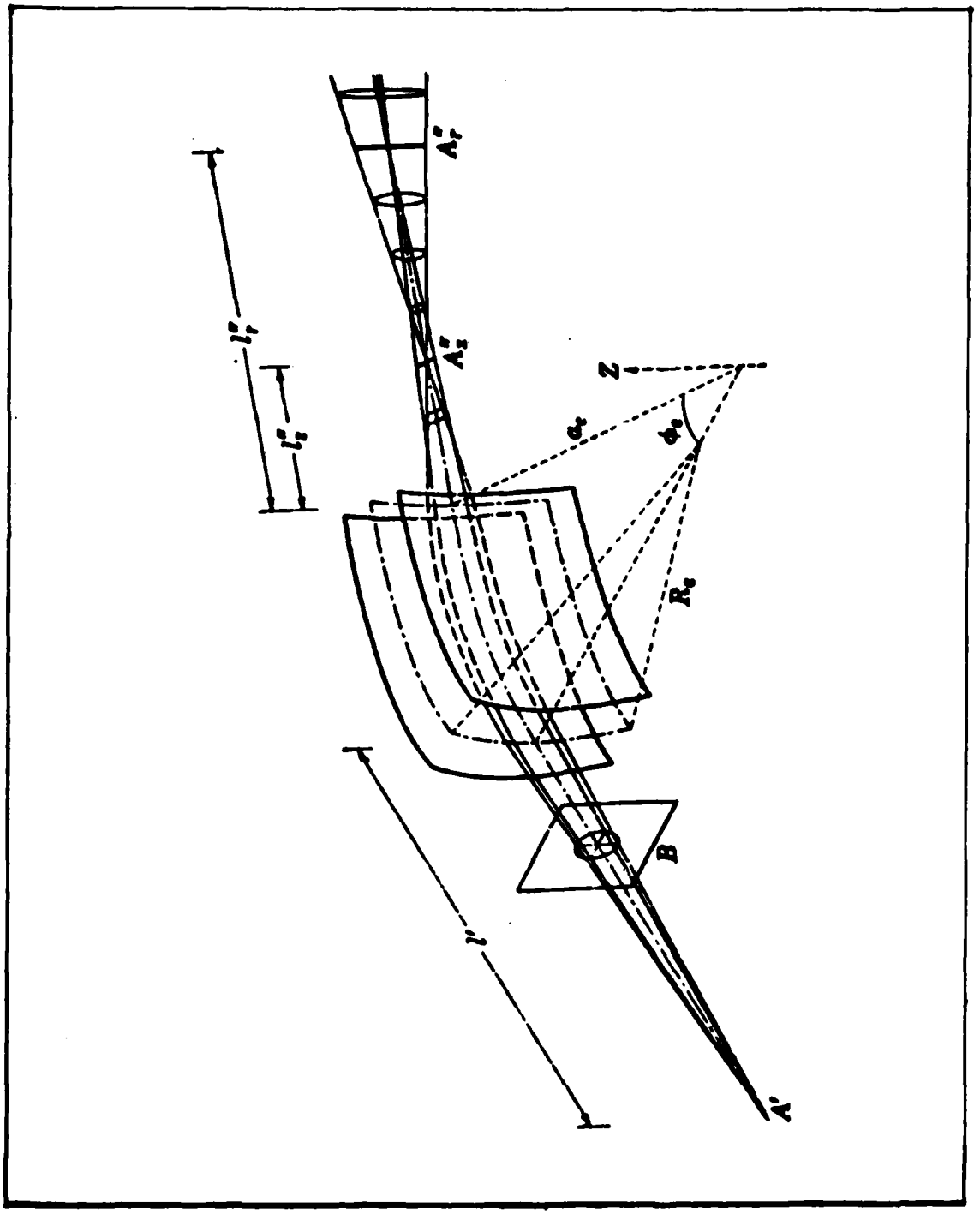

Figure 3 - Mid-Electrode Surface and Object/Image Planes
(From Ewald and Liebl, ref. 2)

appropriate, cylindrical and spherical analyzer formulas will be provided by taking the proper limits of the toroidal analyzer formulas.

Electrostatic analyzers generally have high resolution and high transmission curves, but they are limited to an energy range of about 10 ev to 100 kev. The lower energy limit occurs when the electrode fields are reduced to about the same magnitude as the self-fields of the ion beam. The upper energy limit is due to voltage breakdown across the electrodes.

Electrostatic analyzers are much lighter and have simpler power requirements than do analyzers which use magnets. They are thus well-suited for space applications, such as solar wind experiments. They are also useful in plasma experiments in the laboratory.

B. Problem

Generally, the electrostatic analyzer provides only a single data channel. In certain applications, as in pulsed plasma experiments, there is only a very limited, total observation time. This makes it difficult to gather sufficient data in a single experiment. It is hoped that by extending the cross radius R through a full 2π revolution, that is the radius that sweeps perpendicular to the main ion path (see Figure 2), that an instrument can be designed that provides multiple data channels, each channel sampling a different energy.

C. Coordinate System

The coordinate system that will be employed is the cylindrical coordinate system r, ϕ, z shown in Figures 2 and 3. The radial radii of the electrodes are r_a and r_b. The cross or axial radii of the

electrodes are R_a and R_b. It will be assumed that R_a and R_b have a common center of curvature. The angular extent of the electrodes in the Z = constant plane is $\phi = \phi_e$. The angular extent of the electrodes in the ϕ = constant plane is θ, where θ will be allowed to sweep through a full 2π.

The mid-electrode surface, halfway between the two electrodes, is described by the radii $r = a_e$ and $R = R_e$, as shown in Figure 3. The central path through the electrodes is given by $r = a_e$ and $z = 0$. It will be assumed that the ions enter the electrodes near this central path with small entry angles such that the ions always remain in the close vicinity of the central path.

In most places in this paper, the dimensionless coordinates ρ and ζ will be used where ρ and ζ are defined by

$$\rho = \frac{(r - a_e)}{a_e} \tag{1-4}$$

$$\zeta = \frac{z}{a_e} \tag{1-5}$$

The assumptions in the previous paragraph require that ρ and ζ be much less than one at all times.

D. Approach

The electrostatic equations will be obtained from the literature and modified for use in this paper. Equations of motion will be set up and solved, thus describing the trajectory of an ion through the electrodes. The solutions to the equations of motion will then be manipulated so as to produce optic equations, which provide a more convenient description of the ion behavior. The resolution and

transmission will also be developed at that time. Applications of the optic equations will then be discussed with special attention paid to the behavior of off-center slits. It is the use of off-center slits that permits the analyzer to sample the energy spectra at various points simultaneously, thus providing multiple channels of data.

The trade-offs that are required in designing an actual instrument will then be discussed, with an accent on minimizing the size of the instrument. Design curves involving the various system parameters are presented in the Appendix to assist the reader in designing an instrument suitable to his particular needs.

The effects of errors in the series solutions to the electric fields are discussed with respect to how they impact on the resolution and transmission. The effects of these errors can be minimized with the use of secondary entrance slits which restrict the entrance angles.

Finally, a qualitative discussion is given on the statistical problem of ion flux through the various slits and the electrodes as it relates to the total ion current seen by the detector.

II. Electrostatics

A. Overview

The equations for the radial and axial electric fields, the electrostatic potential, and the equipotential surfaces are listed, as derived by N. Svartholm (Ref 1:196-197). The variables and constants involved are defined and derived. The connection between the voltage, $\pm U_0$, on the electrodes and the central path electric field strength, E_0, is derived. Finally, approximations are made to arrive at the final form of these equations that will be used in subsequent chapters.

B. Electrostatic Equations

As mentioned in the Introduction, the electric field strength equations were obtained from the literature. We will assume that the electric field and the electric potential are both zero outside of the electrodes. Fringing fields will be neglected in this treatment. It will further be assumed that the electrodes are charged to $\pm U_0$ and that the zero equipotential surface is midway between the two electrodes, for small electrode gaps. The electric field is assumed to possess cylindrical symmetry with respect to the z-axis and mirror symmetry with respect to the $z = 0$ plane. If the electric field is given in the $z = 0$ plane near $r = a_e$ by the series expansion

$$E(\rho) = E_0[1 + \beta_1\rho + \beta_2\rho^2 + \beta_3\rho^3 + \ldots] \qquad (2\text{-}1)$$

where $$\rho = \frac{r - a_e}{a_e} \tag{2-2}$$

then according to N. Svartholm (Ref 1:196), the electric potential and the electric field strength in an annulus surrounding $r = a_e$, is given by

$$\begin{aligned} U(\rho,\zeta) = -E_0 a_e [&\rho + \tfrac{1}{2}\beta_1\rho^2 + \tfrac{1}{3}\beta_2\rho^3 + \tfrac{1}{4}\beta_3\rho^4 \\ &- \tfrac{1}{2}(1 + \beta_1)\zeta^2 + \tfrac{1}{2}(1 - \beta_1 - 2\beta_2)\rho\zeta^2 \\ &- \tfrac{1}{2}(1 - \beta_1 + \beta_2 + 3\beta_3)\rho^2\zeta^2 \\ &+ \tfrac{1}{24}(1 - \beta_1 + 4\beta_2 + 6\beta_3)\zeta^4] \end{aligned} \tag{2-3}$$

$$\begin{aligned} E_r(\rho,\zeta) = E_0[&1 + \beta_1\rho + \beta_2\rho^2 + \beta_3\rho^3 \\ &+ \tfrac{1}{2}(1 - \beta_1 + \beta_2 + 3\beta_3)\rho^2\zeta + \tfrac{1}{6}(1 - \beta_1 + 4\beta_2 + 6\beta_3)\zeta^3] \end{aligned} \tag{2-4}$$

$$\begin{aligned} E_z(\rho,\zeta) = E_0[&-(1 + \beta_1)\zeta + (1 - \beta_1 - 2\beta_2)\rho\zeta \\ &- (1 - \beta_1 + \beta_2 + 3\beta_3)\rho^2\zeta \\ &+ \tfrac{1}{6}(1 - \beta_1 - 4\beta_2 + 6\beta_3)\zeta^3] \end{aligned} \tag{2-5}$$

where $$\zeta = \frac{z}{a_e} \tag{2-6}$$

The potential has been set up for $U = 0$, when $r = a_e$, $z = 0$.

When the potential is set to

$$U(\rho,\zeta) = -E_0 a_e \sigma \tag{2-7}$$

where σ is a constant, then the equipotential surface with this particular potential value is given by (Ref 1:197) as

$$\rho = \sigma - \frac{1}{2}\beta_1\sigma^2 + (\frac{1}{2}\beta_1{}^2 - \frac{1}{3}\beta_2)\sigma^3 + \frac{1}{2}[1 + \beta_1 - (1 + \beta_1{}^2 - 2\beta_2)\sigma]\zeta^2 \tag{2-8}$$

The constants β_1 and β_2 are given by H. Ewald and H. Liebl (Ref 2:873) as

$$\beta_1 = -(1 + \frac{a_e}{R_e}) \tag{2-9}$$

$$\beta_2 = 1 + \frac{a_e}{R_e} + a_e{}^2(1 + R_e{}')/2R_e{}^2 \tag{2-10}$$

where

$$R_e{}' \equiv \left.\frac{dR}{dr}\right|_{\substack{r=a_e \\ z=0}} \tag{2-11}$$

In our case, we have

$$R = R_e + (r - a_e) \tag{2-12}$$

therefore,

$$R_e{}' = 1 \tag{2-13}$$

This gives us

$$\beta_2 = 1 + \frac{a_e}{R_e} + \frac{a_e{}^2}{R_e{}^2} \tag{2-14}$$

It appears that Ewald's values for β_1 and β_2 were arrived at by one of his associates, R. Albrecht (Ref:3), who used a general, but difficult, conformal mapping approach involving figures of revolution.

A simpler approach was suggested by H. Wollnik (Ref 4:165-167), for the special case when R_a and R_b are concentric, as is the case here. By symmetry, one can assume that the equipotential surfaces have the same shape as the electrodes. Conservation of electric flux can be used to relate the electric field, E_0, for $r = a_e$, to the electric

field, E, for $r \neq a_e$. This gives us, see figure 2,

$$E(rd\phi)\ (Rd\theta) = E_0(a_e d\phi)\ (R_e d\theta) \tag{2-15}$$

where

$$r = a_e(1 + \rho) \tag{2-16}$$

$$R = R_e + (r - a_e) \tag{2-17}$$

Therefore,

$$E = E_0 \left(\frac{a_e}{r}\right)\left(\frac{R_e}{R}\right) \tag{2-18}$$

or

$$E = E_0\left[\frac{1}{(1 + \rho)}\right]\left[\frac{1}{(1 + \frac{a_e}{R_e}\rho)}\right] \tag{2-19}$$

Equation (2-18) can be written, to second order in ρ, as

$$E = E_0\left[(1 - \rho + \rho^2)\left(1 - \frac{a_e}{R_e}\rho + \frac{a_e^2}{R_e^2}\rho^2\right)\right] \tag{2-20}$$

or

$$E = E_0\left\{1 + \left[-\left(1 + \frac{a_e}{R_e}\right)\right]\rho + \left[1 + \frac{a_e}{R_e} + \frac{a_e^2}{R_e^2}\right]\rho^2\right\} \tag{2-21}$$

This gives us immediately

$$\beta_1 = -\left(1 + \frac{a_e}{R_e}\right) \tag{2-9}$$

$$\beta_2 = \left(1 + \frac{a_e}{R_e} + \frac{a_e^2}{R_e^2}\right) \tag{2-14}$$

These values for β_1 and β_2 are consistent with those given by Ewald. It should be noted equations (2-3), (2-4), and (2-5) apply to either a cylindrical, spherical, or toroidal system. It is the choice of a_e and R_e that determines to which system the equations apply. For the cylindrical system $R_e = \infty$, for the spherical system $R_e = a_e$,

and for the toroidal system most any choice of R_e and a_e is permissible.

C. Electrode Voltage

The voltage, U_0, that is applied plus/minus to the electrodes, is related to the central path electric field strength, E_0, by

$$U_b - U_a = -\int_{\vec{r}_a}^{\vec{r}_b} \vec{E}_0 d\vec{\ell} \tag{2-22}$$

With $U_b = +U_0$, $U_a = -U_0$, and integrating along a radial path in the $\zeta = 0$ plane, we get

$$2U_0 = \int_{\rho_a}^{\rho_b} E\, a_e d\rho \tag{2-23}$$

By using equation (2-19) for the electric field, and setting $\rho_a = -\rho_b$, we arrive at

$$E_0 = \frac{2U_0}{\left\{\frac{a_e}{\left(\frac{a_e}{R_e} - 1\right)} \ln\left[\frac{\left(1 + \frac{a_e}{R_e}\rho_b\right)(1 - \rho_b)}{\left(1 - \frac{a_e}{R_e}\rho_b\right)(1 + \rho_b)}\right]\right\}} \tag{2-24}$$

The electrodes are separated by a distance d, defined by

$$\rho_b = \frac{d}{2a_e} \tag{2-25}$$

E_0, the central path electric field strength, is thus determined by equation (2-24) in terms of the electrode geometry and the applied voltage. To apply it to the spherical case, it is necessary to take the limit as R_e approaches a_e, and to apply L'Hospital's rule.

D. Simplified Electric Field Equations

For the purposes of this thesis, we will need $U(\rho,\zeta)$ only to second order in ρ or ζ, and we will need $E_r(\rho,\zeta)$ and $E_z(\rho,\zeta)$ only to

first order in ρ or ζ. Applying these constraints to equations (2-3), (2-4), (2-5) leaves us with

$$U(\rho,\zeta) = -E_0 a_e\left[\rho + \frac{1}{2}\beta_1\rho^2 - \frac{1}{2}(1 + \beta_1)\zeta^2\right] \tag{2-26}$$

$$E_r(\rho) = E_0[1 + \beta_1\rho] \tag{2-27}$$

$$E_z(\zeta) = E_0[-(1 + \beta_1)\zeta] \tag{2-28}$$

It is these three equations that will be used in the mechanics chapter in the equations of motion.

III. Mechanics

A. Overview

The pattern of development of chapter III closely follows that used by H. E. Duckworth and S. N. Ghoshal (Ref 5:210-221), who will not be further cited. Certain notational changes are made to improve the similarity in form between the radial and axial equations and to generalize the radial solution. The most important change from Duckworth's notation is the transformation of the radial solution to explicitly include the ion energy.

The primary goal of the mechanics chapter is to arrive at solutions for the radial and axial motion of the ions inside of the electrodes. The equations of motion are the standard, cylindrical equations of motion.

By invoking conservation of energy, the centripetal force equation and the electrostatic potential, the velocity change as the ion penetrates the field boundary is derived. This result is coupled with conservation of angular momentum to get a solution for the angular equation of motion.

By combining the solution to the angular equation of motion, centripetal force equation, and the radial electrostatic field, the radial equation of motion can be solved. It is in this section that a connection is made between certain math constants in the radial equation and the energy of the ions, relative to the mean energy, T_0, to which the system is tuned.

By combining the solution to the angular equation, the centripetal force equation, and the axial electric field, the axial equation of motion can be solved, thus completing the mechanics chapter.

B. Equations of Motion

The equations of motion are

$$M\ddot{r} - Mr\dot{\phi}^2 = eE_r \tag{3-1}$$

$$M \frac{d}{dt} (r^2\dot{\phi}) = eE_\phi = 0 \tag{3-2}$$

$$M\ddot{z} = eE_z \tag{3-3}$$

The change of the ion is $e = +1.609 \times 10^{-19}$ coulomb, and the ion mass, M, is defined to be

$$M = M_0(1+\gamma) \tag{3-4}$$

where γ is assumed to be a small number. M_0 will be defined shortly by the centripetal force equation.

C. Velocity Change at Field Boundary

For an ion of mass, M, and a velocity

$$v' = v_0(1+\beta) \tag{3-5}$$

outside the electric field, with β assumed to be a small number, the velocity, v, of the ion just after it enters the field is given by the energy balance equation,

$$\frac{1}{2} M(v'^2) = \frac{1}{2} Mv^2 + eU \tag{3-6}$$

This can be rearranged as

$$v = \sqrt{(v')^2 - \frac{2EU}{M}} \tag{3-7}$$

For an ion of mass M_0 and velocity v_0 undergoing pure angular motion in the field along $\rho = o$ and $z = 0$, the centripetal force equation is

$$\vec{f}_c = \frac{-M_0 v_0^2}{a_e} \hat{r} = \vec{F}_e = eE_0\hat{r} \tag{3-8}$$

This gives

$$eE_0 a_e = -M_0 v_0^2 \tag{3-9}$$

By combining equations (2-9), (2-26), (3-4), (3-5), (3-7), (3-9), rearranging, and expanding to second order in ρ, ζ, β, or γ, we arrive at

$$v = v_0\left[1+\beta-\rho+\frac{1}{2}\left(\frac{a_e}{R_e}\right)(\rho^2-\zeta^2)+\rho\left(\frac{\beta}{2}+\gamma\right)\right] \tag{3-10}$$

This is the velocity, v, of an ion in the field that started with a velocity, $v' = v_0(1+\beta)$, outside of the field. Equation (3-10) will also be needed to first order:

$$v = v_0(1+\beta-\rho) \tag{3-11}$$

D. Angular Equation of Motion

The ion velocity component along the central path is the angular velocity, v_ϕ, which is given by

$$v_\phi = v\cos(\quad) \tag{3-12}$$

where σ_1 is the angle between the ion path and the central path. v is the ion velocity inside the field after it enters at the point (ρ_1,ζ_1).

Since the entrance angles were assumed to be small, we can use the approximation, $\cos(\sigma_1) = 1 - \frac{1}{2}\sigma_1^2$. By combining this with the equations for v, (3-10), and for v_ϕ, (3-12), expanding and retaining only second order terms in β, γ, ρ_1, and ζ_1, we have

$$v_\phi = v_0\left[1+\beta-\rho_1+\frac{1}{2}\left(\frac{a_e}{R_e}\right)(\rho_1^2-\zeta_1^2)+\rho_1\left(\frac{\beta}{2}+\gamma\right)-\frac{1}{2}\sigma_1^2\right] \qquad (3\text{-}13)$$

We can also write

$$\dot{\phi}_1 = \frac{v}{r_1} = \frac{v}{a_e(1+\rho_1)} \qquad (3\text{-}14)$$

We thus have

$$\dot{\phi}_1 = \frac{v_0}{a_e}\left[1+\beta-2\rho_1-\frac{1}{2}\beta\rho_1+\gamma\rho_1+2\rho_1^2+\frac{1}{2}\left(\frac{a_e}{R_e}\right)(\rho_1^2-\zeta_1^2)-\frac{1}{2}\sigma_1^2\right] \qquad (3\text{-}15)$$

The second equation of motion gives us conservation of angular momentum, from which we can write

$$r^2\dot{\phi} = r_1^2\dot{\phi}_1 \qquad (3\text{-}16)$$

By substituting the equation for $\dot{\phi}_1$, (3-15), into equation (3-16) and solving for $\dot{\phi}$ to second order in β, γ, ρ, ρ_1, ζ_1, and σ_1, we arrive at

$$\dot{\phi} = \frac{v_0}{a_e}\left[1+\beta-2\rho-2\rho\beta+3\rho^2-\rho_1^2+\frac{3}{2}\beta\rho_1+\rho_1\gamma-\frac{1}{2}\sigma_1^2+\frac{1}{2}\left(\frac{a_e}{R_e}\right)(\rho_1^2-\zeta_1^2)\right] \qquad (3\text{-}17)$$

This equation describes the angular motion of an ion, but it is nonlinear and coupled. The $\dot{\phi}$ equation was derived to second order only to keep from losing first order terms. To first order, the $\dot{\phi}$ equation is

$$\dot{\phi} = \frac{v_0}{a_e}(1+\beta-2\rho) \qquad (3\text{-}18)$$

This equation for $\dot{\phi}$ will be used in the radial equation of motion. It will also be useful to drop the $\dot{\phi}$ equation to zeroth order and integrate with respect to time.

$$\phi = \frac{v_0 t}{a_e} \tag{3-19}$$

This equation will be useful later in eliminating (t), from the radial and axial solutions, in favor of (ϕ).

E. Radial Equation of Motion

As $r = a_e(1+\rho)$, we have $\ddot{r} = a_e\ddot{\rho}$; therefore, the radial equation of motion (3-1) can be transformed to

$$Ma_e\ddot{\rho} - Ma_e(1+\rho)\,(\dot{\phi})^2 = eE\rho \tag{3-20}$$

By combining the equations for β_1 (2-9), $E\rho$ (2-27), M (3-4), the centripetal force (3-9), and $\dot{\phi}$ (3-18), with the radial equation (3-20), we arrive, to first order in β, γ, and ρ, at

$$\ddot{\rho} = \left(\frac{v_0}{a_e}\right)^2 \left[(\gamma+2\beta) - \rho\left(2-\frac{a_e}{R_e}\right)\right] \tag{3-21}$$

By defining the following three new constants

$$\varepsilon^2 = \frac{a_e}{R_e} \tag{3-22}$$

$$\chi^2 = 2 - \varepsilon^2 \tag{3-23}$$

$$\delta = \frac{\gamma + 2\beta}{\chi^2} \tag{3-24}$$

we can transform the radial equation of motion to its final form shown below

$$\ddot{\rho} + \chi^2\left(\frac{v_0}{a_e}\right)^2\rho = \chi^2\left(\frac{v_0}{a_e}\right)^2\delta \tag{3-25}$$

The particular solution is obviously $\rho_p = \delta$. The homogeneous solution depends on the value of χ^2. For $\chi^2 = 0$

$$\rho_h(t) = A_1^* t + B_1 \tag{3-26}$$

We can eliminate (t) in favor of (ϕ) with the aid of equation (3-19). By defining $A_1 = A_1^* \frac{a_e}{v_0}$, we have

$$\rho_h(\phi) = A_1\phi + B_1 \tag{3-27}$$

Therefore,

$$\rho(\phi) = A_1\phi + B_1 + \delta \tag{3-28}$$

For $\chi^2 > 0$, we have

$$\rho_h(t) = A_2\cos\left(\chi\frac{v_0}{a_e}t\right) + B_2\sin\left(\chi\frac{v_0}{a_e}t\right) \tag{3-29}$$

Therefore,

$$\rho(\phi) = A_2\cos(\chi\phi) + B_2\sin(\chi\phi) + \delta \tag{3-30}$$

For $\chi^2 < 0$, we have

$$\rho(\phi) = A_3\cosh(\chi\phi) + B_3^*\sinh(\chi\phi) + \delta \tag{3-31}$$

Since $\chi^2 < 0$, χ is purely imaginary. We can then define χ^* as follows, with $\hat{i} = \sqrt{-1}$,

$$\hat{i}\chi^* = \hat{i}\sqrt{\epsilon^2-2} = \chi \tag{3-32}$$

By defining $B_3 = \hat{i}B_3^*$, the third solution becomes

$$\rho(\phi) = A_3\cos(\chi^*\phi) + B_3\sin(\chi^*\phi) + \delta \tag{3-33}$$

By redefining χ^2 to be

$$\chi^2 = |2 - \epsilon^2| \tag{3-34}$$

then $\chi^* = \chi$, and the third solution becomes identical in form to the second solution.

The boundary conditions are declared to be

$$\rho(0) = \rho_1 \tag{3-35}$$

$$\left.\frac{d\rho}{d\phi}\right|_{\phi=0} = -\alpha_r' \tag{3-36}$$

where α_r' will be defined later in the optics chapter as the radial entry angle. Applying these conditions gives us

$$\chi^2 = 0 \qquad \rho(\phi) = -\alpha_r'\phi + \rho_1 \tag{3-37}$$

$$\chi^2 \neq 0 \qquad \rho(\phi) = (\rho_1-\delta)\cos(\chi\phi) - \frac{\alpha_r'}{\chi}\sin(\chi\phi) + \delta \tag{3-28}$$

In the limit as $\chi^2 \to 0$, the solution for $\chi^2 \neq 0$ reduces to the $\chi^2 = 0$ solution. It is thus seen that the trig solution (3-38) contains both the linear solution and the hyperbolic solution.

The parameter δ can be related to the kinetic energy of the ion. We can define T to be the energy of an ion outside the field with mass M and velocity v', and T_0 to be the kinetic energy of an ion of mass M_0 and velocity v_0. Therefore, we have

$$T = \frac{1}{2}M(v')^2 = \frac{1}{2}M_0(1+\gamma){v_0}^2(1+\beta)^2$$

$$= T_0(1+\gamma)\ (1+\beta)^2 \tag{3-39}$$

To first order in β and γ, we have

$$T = T_0(1 + 2\beta + \gamma)$$

By applying the definition for δ (3-24), we have

$$T = T_0(1 + \chi^2\delta) \tag{3-40}$$

Solving for δ gives us

$$\delta = \frac{1}{\chi^2}\left(\frac{T - T_0}{T_0}\right) \tag{3-41}$$

By defining the relative energy, η, as

$$\eta = \frac{T - T_0}{T_0} \tag{3-42}$$

we have

$$\delta = \frac{\eta}{\chi^2} \tag{3-43}$$

It should be noted that T is the unperturbed kinetic energy of an ion outside of the electrostatic field, whereas T_0 is the kinetic energy of an ion inside the field. Specifically, T_0 is the kinetic energy to which the analyzer is tuned. It is this energy that will permit an ion to track the central path through the electrodes.

By substituting this expression for δ (3-42) into equation (3-38), we arrive at the final form of the radial solution:

$$\rho = \left(\rho_1 - \frac{\eta}{\chi^2}\right)\cos(\chi\phi) - \frac{\alpha_r'}{\chi}\sin(\chi\phi) + \frac{\eta}{\chi^2} \tag{3-44}$$

This form of the radial solution is in terms of the relative ion energy, the point of entry, the entry angle, and the electrode geometry.

F. Axial Equation of Motion

As $z = a_e\zeta$, we have $\ddot{z} = a_e\ddot{\zeta}$; therefore, the axial equation of motion (3-3) can be transformed to

$$Ma_e\ddot{\zeta} = eE_\zeta \tag{3-45}$$

By combining the equations for β_1 (2-9), E_ζ (2-28), M (3-4), and the centripetal force (3-9), with the axial equation (3-44), we arrive, to first order in β, γ, and ζ, at

$$\ddot{\zeta} + \left(\frac{v_0\epsilon}{a_e}\right)^2\zeta = 0 \tag{3-46}$$

The standard solution to this equation is

$$\zeta(t) = A\cos\left(\epsilon\frac{v_0 t}{a_e}\right) + B\sin\left(\epsilon\frac{v_0 t}{a_e}\right) \tag{3-47}$$

By invoking the equation for ϕ (3-19), we have

$$\zeta(\phi) = A\cos(\epsilon\phi) + B\sin(\epsilon\phi) \tag{3-48}$$

The boundary conditions are declared to be

$$\zeta(0) = \zeta_1 \tag{3-49}$$

$$\left.\frac{d\zeta}{d\phi}\right|_{\phi=0} = -\alpha_z' \tag{3-50}$$

where α_z' will be defined later in the optics chapter as the axial entry angle. Applying these conditions, we arrive at

$$\zeta(\phi) = \zeta_1\cos(\epsilon\phi) - \frac{\alpha_z'}{\epsilon}\sin(\epsilon\phi) \tag{3-51}$$

This form of the axial solution is in terms of the point of entry, the entry angle, and the electrode geometry. It differs in form from the radial solution only in that the relative energy does not appear

in the axial solution. This difference is principally connected to the fact that the axial electric field is much smaller than the radial electric field.

G. Summary of Key Mechanics Equations

For the convenience of the reader, certain key mechanics equations which will be needed in the optics chapter are listed here for future reference.

$$\epsilon^2 = \frac{a_e}{R_e} \tag{3-22}$$

$$\chi^2 = |2 - \epsilon^2| \tag{3-34}$$

$$\eta = \frac{T - T_0}{T_0} \tag{3-42}$$

$$\rho(\phi) = \left(\rho_1 - \frac{\eta}{\chi^2}\right) \cos(\chi\phi) - \frac{\alpha_r'}{\chi} \sin(\chi\phi) + \frac{\eta}{\chi^2} \tag{3-44}$$

$$\zeta(\phi) = \zeta_1 \cos(\epsilon\phi) - \frac{\alpha_z'}{\epsilon} \sin(\epsilon\phi) \tag{3-51}$$

IV. Optics

A. Overview

The pattern of development of chapter IV closely follows that used by H. E. Duckworth and S. N. Ghoshal (Ref 5:210-221), who will not be further cited. Many of the toroidal equations presented in this chapter were developed in analogy to the cylindrical equations produced by Duckworth and Ghoshal. Certain notational changes, consistent with chapter III, are made to improve the similarity in form between the radial and axial equations and to permit the equations to explicitly contain the relative ion energy.

In this chapter, coordinate systems are established in the regions outside the entrance and exit to the electrodes. The behavior of the ions in these regions is worked out and refraction at the field boundary is considered.

By combining the behavior of the ions outside the electrodes with the solutions to the radial and axial equations of motion inside the electrodes, the locations of the radial and axial image planes are determined.

Further manipulation of the equations which specify the locations of the image planes yields the location of the radial and axial focal points, the radial and axial "focal lengths," and the radial and axial Newtonian lens equations. It must be remembered that, while these equations are patterned after the thin optical lens equations, the electrostatic analyzer is not a thin optical lens and thus, some of the

results in the applications chapter (chapter V) are different from what one might first expect.

By comparing post-electrode ion locations with pre-electrode starting points, the radial and axial image magnifications, the energy dispersion, the resolution, and the transmission are calculated.

B. Entrance Coordinate System

The space outside of the electrodes is assumed to be field-free, thus the ion trajectories are straight lines. Cartesian coordinate systems are therefore a natural choice for describing the motion of the ions as they approach or leave the electrodes.

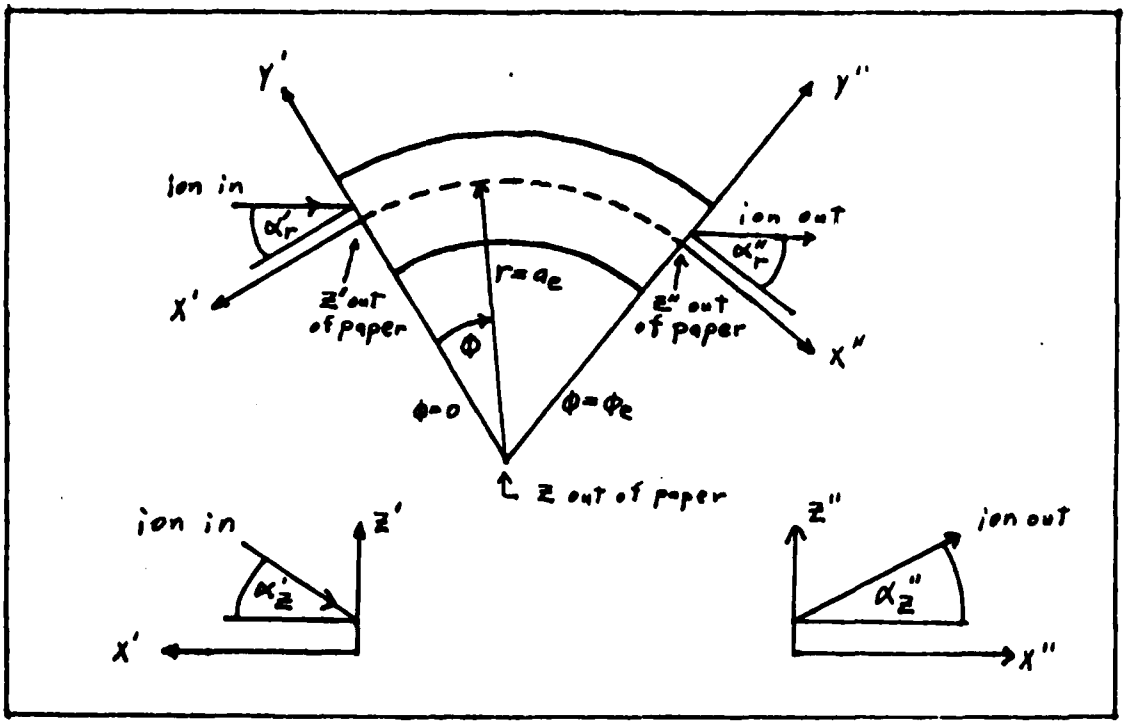

Figure 4 - Entrance/Exit Coordinate Systems

At the entrance, $\phi = 0$, the coordinates are x', y', z' with the origin located at $\rho = 0$, $\zeta = 0$, $\phi = 0$ (see Figure 4). The positive x'-direction points away from the electrodes; thus, at the origin

$dx' = -a_e d\phi$. The positive y'-direction matches the positive r or ρ-direction; thus, at the field boundary $dy' = dr = a_e d\rho$. The positive z'-direction matches the positive z or ζ-direction; thus, at the field boundary $dz' = dz = a_e d\zeta$.

The angle α_r' is defined to be the angle between the x'-axis and the projection of the ion path onto the x'y'-plane (see Figure 4). It should be noted that if $\alpha_r' > 0$, evaluated at the field boundary, then ρ is decreasing. This is because the ion is moving in the (-x') direction.

The angle α_z' is defined to be the angle between the x'-axis and the projection of the ion path onto the x'z'-plane (see Figure 4). It should be noted that if $\alpha_z' > 0$, evaluated at the field boundary, then ζ is decreasing. As in the radial case, this is because the ion is moving in the (-x') direction.

The angles α_r' and α_z' will both be assumed to be small angles. This is required in order to be consistent with the earlier assumption in the electrostatics chapter that the ion path must remain in the close vicinity of the central path through the electrodes. With the assumption of small angles, we can write

$$\left.\frac{-d\rho}{d\phi}\right|_{\phi=0} = \left.\frac{dy'}{dx'}\right|_{x'=0} = \tan(\alpha_r') \simeq \alpha_r' \qquad (4\text{-}1)$$

$$\left.\frac{-d\zeta}{d\phi}\right|_{\phi=0} = \left.\frac{dy'}{dx'}\right|_{x'=0} = \tan(\alpha_z') \simeq \alpha_z' \qquad (4\text{-}2)$$

This establishes the connect between α_r' and α_z' with the boundary conditions (3-36), (3-50) used in the mechanics chapter.

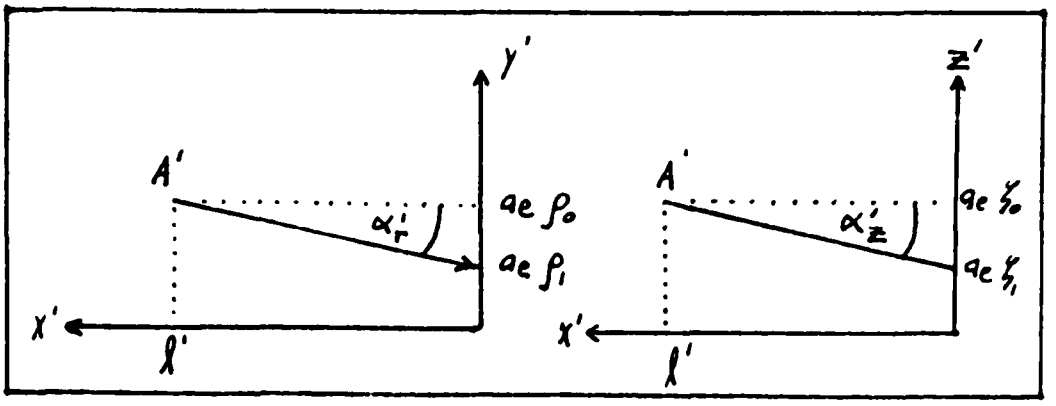

Figure 5 - Entrance Angles

By the use of simple geometry, we can arrive at expressions for α_r' and α_z' in terms of the coordinates. Let us assume that the ion originated from the off-axis point A' with the coordinates $x' = \ell'$, $y' = a_e\rho_0$, $z' = a_e\zeta_0$ (see Figure 5). Let us further assume that the ion enters the field at a point with the coordinates $x' = 0$, $y' = a_e\rho_1$, $z' = a_e\zeta_1$. From the geometry, it is apparent that

$$\tan(\alpha_r') \simeq \alpha_r' = \frac{a_e}{\ell'}(\rho_0 - \rho_1) \qquad (4\text{-}3)$$

$$\tan(\alpha_z') \simeq \alpha_z' = \frac{a_e}{\ell'}(\zeta_0 - \zeta_1) \qquad (4\text{-}4)$$

Equations (4-3) and (4-4) will permit the eventual elimination of α_r' and α_z', in favor of the coordinates of the ion source and the coordinates of the ion's point of entry into the electric field.

C. Exit Coordinate System

The exit coordinate system x", y", z" has its origin located at $\rho = 0$, $\zeta = 0$, $\phi = \phi_e$ (see Figure 4). The positive x"-direction points away from the electrodes, but this time it is in the direction of the ion motion; thus, at the origin $dx'' = +a_e d\phi$. The positive y" and

z"-directions match up with the positive ρ and ζ-directions respectively; thus, at the field boundary $dy'' = a_e d\rho$ and $dz'' = a_e d\zeta$.

The angle α_r'' is defined to be the angle between the x"-axis and the projection of the ion path onto the x"y"-plane. As the ion is now moving in the direction of increasing x", the angle $\alpha_r'' > 0$ corresponds to increasing ρ.

The angle α_z'' is defined to be the angle between the x"-axis and the projection of the ion path onto the x"z"-plane. We now have (similar to the radial case) $\alpha_z'' > 0$ corresponding to increasing ζ.

We will assume that α_r'' and α_z'' are small angles. This is consistent with the assumption that α_r' and α_z' are small angles and with time reversal symmetry. With the assumption of small angles, we can write

$$\left.\frac{d\rho}{d\phi}\right|_{\phi=\phi_e} = \left.\frac{dy''}{dx''}\right|_{x''=0} = \tan(\alpha_r'') \simeq \alpha_r'' \qquad (4\text{-}5)$$

$$\left.\frac{d\zeta}{d\phi}\right|_{\phi=\phi_e} = \left.\frac{dz''}{dx''}\right|_{x''=0} = \tan(\alpha_z'') \simeq \alpha_z'' \qquad (4\text{-}6)$$

By using the equations for ρ (3-44) and for ζ (3-51), we can evaluate the differentials in expressions for α_r'' and α_z'' as

$$\alpha_r'' = \left.\frac{d\rho}{d\phi}\right|_{\phi=\phi_e} = -\chi\left(\rho_1 - \frac{\eta}{\chi^2}\right)\sin(\chi\phi_e) - \alpha_r' \cos(\chi\phi_e) \qquad (4\text{-}7)$$

$$\alpha_z'' = \left.\frac{d\zeta}{d\phi}\right|_{\phi=\phi_e} = -\varepsilon\zeta_1 \sin(\varepsilon\phi_e) - \alpha_z' \cos(\varepsilon\phi_e) \qquad (4\text{-}8)$$

This gives us α_r'' and α_z'' in terms of the entry angles, the electrode geometry, and the coordinates of the ion's point of entry into the

electric field. We will need α_r'' and α_z'' shortly to compute the ion motion after it exits from the electrodes.

D. Refraction at Field Boundary

It would be apropos to investigate the effect of ion path bending or refraction at the field boundary at this point before continuing.

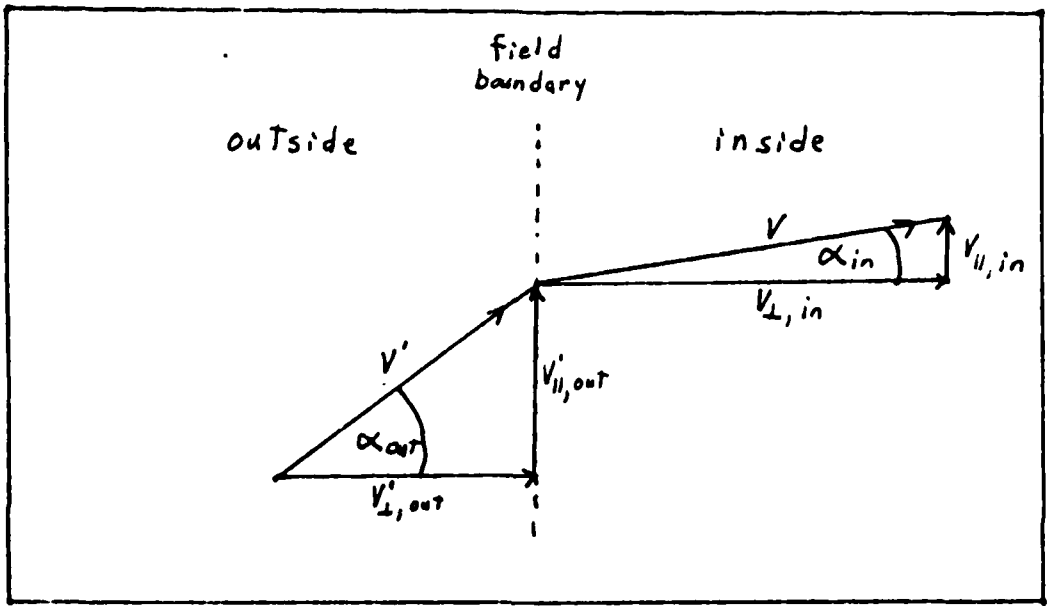

Figure 6 - Electrostatic Snell's Law

For an ion penetrating a boundary with a finite potential change, the velocity component parallel to the boundary, $V_{\parallel}$, is essentially unchanged. It is the velocity component perpendicular to the boundary, $V_{\perp}$, that is affected by the change in potential energy (Ref 5:173). We thus have (see Figure 6) outside the boundary, $\sin(\alpha_o) = V_{\parallel}/V_{\perp o}$, and inside the boundary, $\sin(\alpha_i) = V_{\parallel}/V_{\perp i}$. Solving these two equations for $V_{\parallel}$ and equating them gives us an electrostatic Snell's law:

$$V_{\perp o} \sin(\alpha_o) = V_{\perp i} \sin(\alpha_i) \qquad (4\text{-}9)$$

or for small angles

$$V_{\perp o}\,\alpha_o = V_{\perp i}\,\alpha_i \tag{4-10}$$

We can equate $V_{\perp o}$ to V' (3-5), α_o to α_r' (4-3), and $V_{\perp i}$ to V (3-11) with $\rho = \rho_1$. We therefore have

$$V'\alpha_r' = V\alpha_i \tag{4-11}$$

or

$$V_o(1+\beta)\,\frac{a_e}{\ell'}\,(\rho_o - \rho_1) = V_o(1+\beta-\rho_1)\alpha_i \tag{4-12}$$

Solving for α_i to first order in β, ρ_o and ρ_1, we have

$$\alpha_i = \frac{a_e}{\ell'}\,(\rho_o - \rho_1)$$

$$= \alpha_r' \tag{4-13}$$

By exact analogy, we also have in the axial case, $\alpha_i = \alpha_z'$, where α_i is now an axial angle instead of a radial angle. Thus to first order, we may ignore any ion refraction at the field boundary. This is true at both the entrance or the exit.

Refraction could not be ignored in any study which was interested in examining higher-order effects, such as image aberrations. To get some feel for the effect of the higher order terms, we start again with the electrostatic Snell's law (4-9). By assuming that the angles are small, we can replace the sine function in equation (4-9) with the tangent function:

$$V_{\perp o}\,\tan(\alpha_o) = V_{\perp i}\,\tan(\alpha_i) \tag{4-14}$$

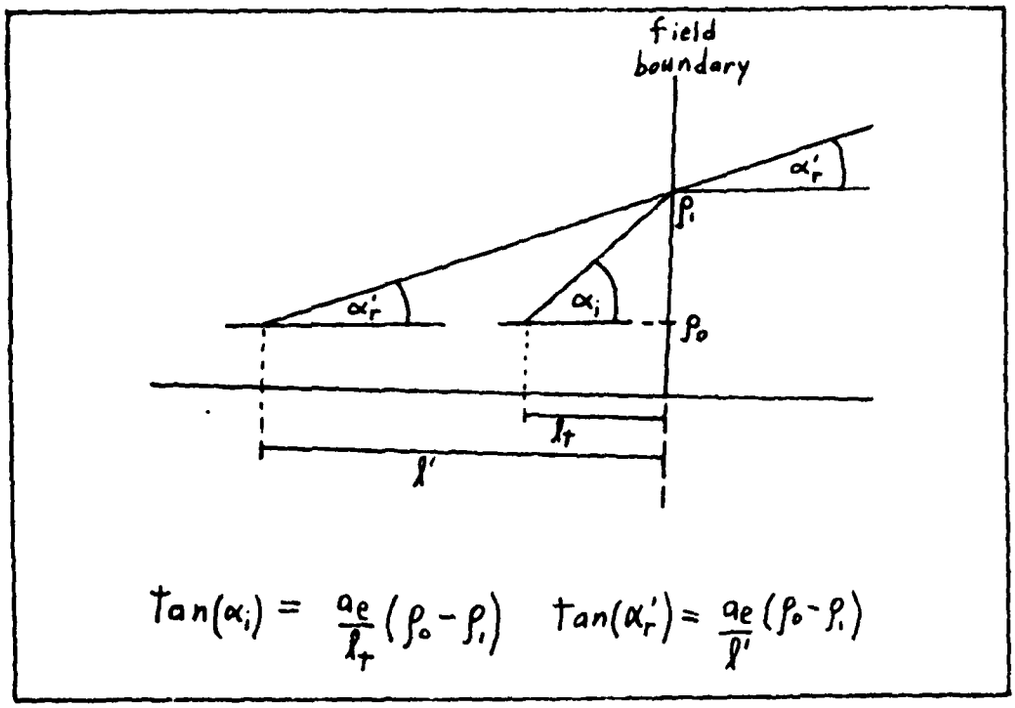

Figure 7 - Refraction at Field Boundary

We can equate $V_{\perp o}$ to V' (3-5), α_o to α_r' (4-3), and $V_{\perp i}$ to V (3-10) with $\rho = \rho_1$, $\zeta = 0$. By replacing tan (α_r') and tan (α_i) with the formulas shown in Figure 7, we can solve for ℓ_t/ℓ' to get, to second order in β, ρ_o, ρ_1,

$$\frac{\ell_t}{\ell'} = \frac{\left(1 + \beta - \rho_1 + \rho_1^2 + \frac{1}{2}\rho_1\beta\right)}{(1 + \beta)} \qquad (4\text{-}15)$$

In the rest of this paper, the refraction will be ignored, and ℓ' will be used to identify the x'-distance to the ion source. If we did want to investigate the second order effects of refraction, we would have to replace ℓ' with ℓ_t, as calculated by equation (4-15). This equation has been graphed in Figure 8 on the next page.

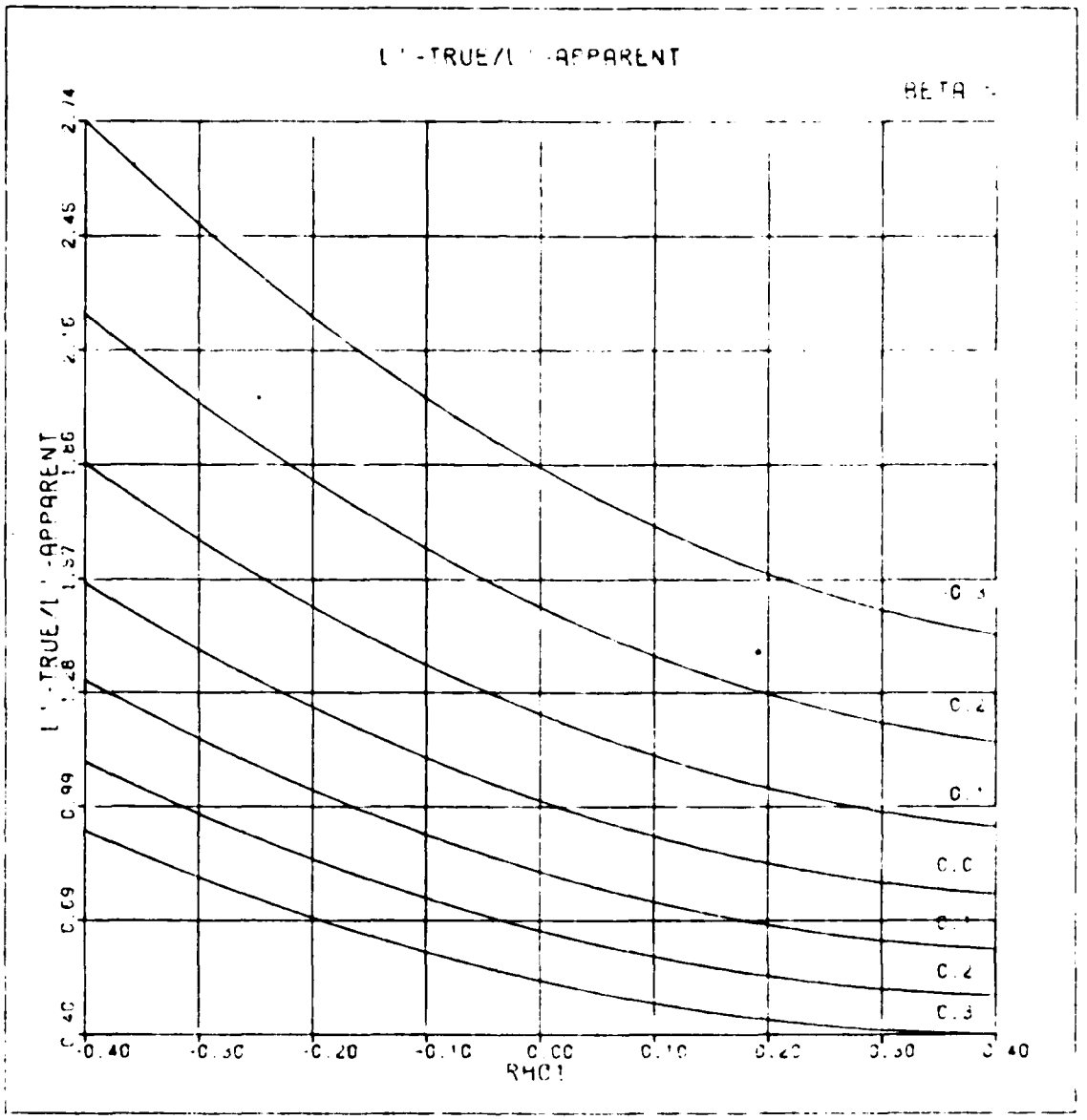

Figure 8 - True versus Apparent Source

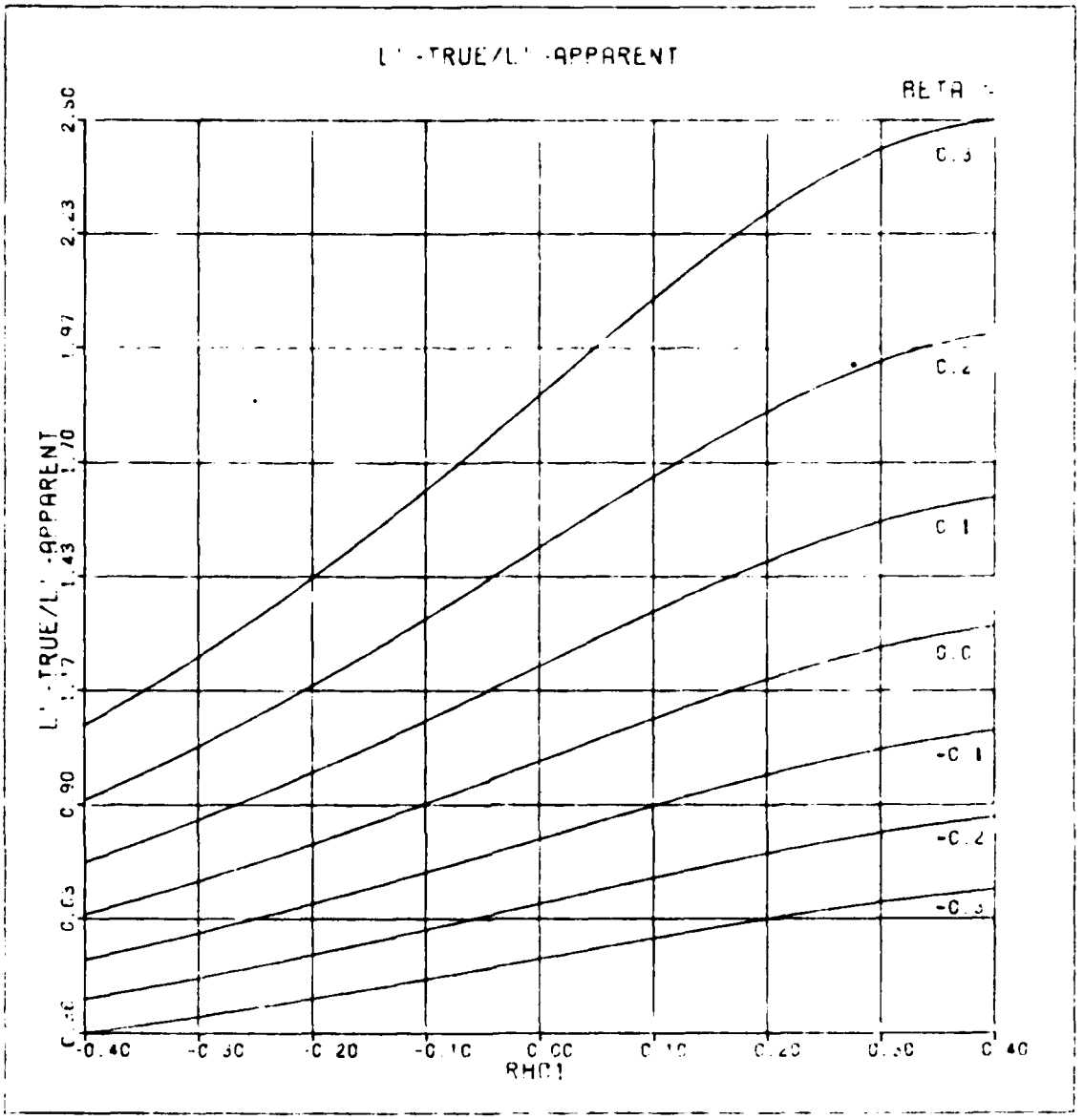

Figure 9 - True versus Apparent Radial Image Plane

Of greater interest is the effect of refraction on the image location. By applying an equation that will be developed later, the radial Newtonian lens equation ($g_r = 0$, $\ell_r'' = \ell'$), we get

$$\frac{\ell_{rt}''}{\ell_r''} = \frac{(1 + \beta)}{\left(1 + \beta - \rho_1 + \rho_1^2 + \frac{1}{2}\rho_1\beta\right)} \qquad (4\text{-}16)$$

ℓ_r'' is the radial image location that will be derived later, assuming no refraction. ℓ_{rt}'' is the radial image location when refraction is considered. Figure 9, on the previous page, shows equation (4-16) graphed for several values of β. The ion energy T is greater than/less than T_0 as β is greater than/less than zero.

Figure 9 shows that ions with an energy $T < T_0$ tend to focus in a shorter distance than those ions with $T > T_0$. Figure 9 also shows that ions with an entry point such that $\rho_1 > 0$ are focused farther out than those ions with $\rho_1 < 0$. Just exactly where an ion ends up depends on its particular values of T and ρ_1. In general, as the ion energy deviates from T_0 and the entry point varies from $\rho_1 = 0$; the ion image changes to a new location. If the exit slit is located at ℓ_r'', then the refraction effects lead to a loss of ions. Along $\rho_1 = 0$, the error in the image location is slightly stronger for $T < T_0$ than it is for $T > T_0$. These effects distort both the transmission curve and the resolution. While these effects are definitely of interest, for purposes of this study, they will be ignored in the rest of this paper.

E. Radial Image Location

From Figure 4, it can be seen that the y'' coordinate of an ion after it exits the electrodes is given by

$$y''(x'') = y''(0) + x'' \tan(\alpha_r'') \qquad (4\text{-}17)$$

or for small angles

$$y''(x'') = y''(0) + x''\alpha_r'' \tag{4-18}$$

At $x'' = 0$, we can equate $y''(0)$ with $a_e\rho(\phi_e)$. We can thus combine the above equation (4-18) with the equation for ρ (3-44) evaluated at $\phi = \phi_e$, the equation for α_r'' (4-7), and the equation for α_r' (4-3), to get

$$\begin{aligned} y''(x'') = \eta&\left[\frac{-a_e}{\chi^2}\cos(\chi\phi_e) + \frac{a_e}{\chi^2} + \frac{x''}{\chi}\sin(\chi\phi_e)\right] \\ &-\rho_0\left[\frac{a_e}{\chi\ell'}\sin(\chi\phi_e) + \frac{a_e x''}{\ell'}\cos(\chi\phi_e)\right] \\ &+\rho_1\left[a_e\left(1 + \frac{x''}{\ell'}\right)\cos(\chi\phi_e) + \left(\frac{a_e^2}{\chi\ell'} - x''\chi\right)\sin(\chi\phi_e)\right] \end{aligned} \tag{4-19}$$

It is desirable that all of the ions of a given energy, that originate from one given point A', be focused at the same point A_r'' after they exit the electrodes. This is possible if and only if the coefficient of ρ_1 in equation (4-19) vanishes. By setting the coefficient of ρ_1 to zero, we can solve it for x", thus determining the location ℓ_r'' of the radial image plane in terms of the other system parameters. This gives us

$$x'' \equiv \ell_r'' = \frac{\left[\frac{a_e^2}{\chi^2} + \frac{a_e\ell'}{\chi}\cot(\chi\phi_e)\right]}{\left[\ell' - \frac{a_e}{\chi}\cot(\chi\phi_e)\right]} \tag{4-20}$$

F. Axial Image Location

Similar to the radial case, the Z" coordinate of an ion after it exits the electrodes is given by

$$Z''(X'') = Z''(0) + X''\tan(\alpha_z'') \tag{4-21}$$

or for small angles

$$Z''(X'') = Z''(0) + X'' \alpha_z'' \tag{4-22}$$

At $X'' = 0$, we can equate $Z''(0)$ with $a_e\zeta(\phi_e)$. We can thus combine the above equation (4-22) with the equation for ζ (3-51) evaluated at $\phi = \phi_e$, the equation for α_z'' (4-8), and the equation for α_z' (4-4), to get

$$Z''(X'') = -\zeta_0\left[\frac{a_e^2}{\epsilon\ell'}\sin(\epsilon\phi_e) + \frac{a_e X''}{\ell'}\cos(\epsilon\phi_e)\right]$$
$$+\zeta_1\left[a_e\left(1 + \frac{x''}{\ell'}\right)\cos(\epsilon\phi_e) + \left(\frac{a_e^2}{\epsilon\ell'} - x''\epsilon\right)\sin(\epsilon\phi_e)\right] \tag{4-23}$$

As in the radial case, we desire that all of the ions of a given energy, that originate from one given point A', be focused at the same point A_z'' after they exit the electrodes. This is possible if and only if the coefficient of ζ_1 in equation (4-23) vanishes. By setting the coefficient of ζ_1 to zero, we can solve it for x", thus determining the location ℓ_z'' of the axial image plane in terms of the other system parameters. This gives us

$$x'' \equiv \ell_z'' = \frac{\left[\frac{a_e^2}{\epsilon^2} + \frac{a_e\ell'}{\epsilon}\cot(\epsilon\phi_e)\right]}{\left[\ell' - \frac{a_e}{\epsilon}\cot(\epsilon\phi_e)\right]} \tag{4-24}$$

Note the extreme similarity of form of the axial equation (4-24) with the radial equation (4-20). This will occur often as we proceed with the Optics chapter.

G. Radial and Axial Focal Points

It is of interest to know where a parallel beam of ions into the system will be focused. This is easily obtained by taking the limit of ℓ_r'' and ℓ_z'' as ℓ' goes to infinity. From equations (4-20) and (4-24), we have

$$g_r'' \equiv \lim_{\ell' \to \infty} \ell_r'' = \frac{a_e}{\chi} \cot(\chi\phi_e) \tag{4-25}$$

$$g_z'' \equiv \lim_{\ell' \to \infty} \ell_z'' = \frac{a_e}{\varepsilon} \cot(\varepsilon\phi_e) \tag{4-26}$$

The locations of the radial and the axial focal points are g_r'' and g_z'' respectively.

It is also of interest to know what ℓ' would have to be in order to provide for a parallel beam of ions out of the system. In this case ℓ_r'' and ℓ_z'' separately would be equal to infinity. Solving equations (4-20) and (4-24) for ℓ' (now called ℓ_r' and ℓ_z' respectively), we get

$$\ell_r' = \frac{\frac{a_e^2}{\chi^2} + \frac{a_e}{\chi}\ell_r'' \cot(\chi\phi_e)}{\ell_r'' - \frac{a_e}{\chi}\cot(\chi\phi_e)} \tag{4-27}$$

$$\ell_z' = \frac{\frac{a_e^2}{\varepsilon^2} + \frac{a_e}{\varepsilon}\ell_z'' \cot(\varepsilon\phi_e)}{\ell_z'' - \frac{a_e}{\varepsilon}\cot(\varepsilon\phi_e)} \tag{4-28}$$

Taking the limits as ℓ_r'' and ℓ_z'' go to infinity gives us

$$g_r' \equiv \lim_{\ell_r'' \to \infty} \ell_r' = \frac{a_e}{\chi} \cot(\chi\phi_e) \tag{4-29}$$

$$g_z' \equiv \lim_{\ell_z'' \to \infty} \ell_z' = \frac{a_e}{\varepsilon} \cot(\varepsilon\phi_e) \tag{4-30}$$

As expected, for reasons of symmetry, we have $g_r' = g_r'' \equiv g_r$ and $g_z' = g_z'' \equiv g_z$. Thus the focal points (measured from the ends of the electrodes) are located at

$$g_r = \frac{a_e}{\chi} \cot(\chi\phi_e) \tag{4-31}$$

$$g_z = \frac{a_e}{\epsilon} \cot(\epsilon\phi_e) \tag{4-32}$$

H. Newtonian Lens Equations

Substituting g_r (4-31) and g_z (4-32) into the equations for ℓ_r'' (4-20) and ℓ_z'' (4-24) gives us

$$\ell_r'' = \frac{\frac{a_e^2}{\chi^2} + \ell' g_r}{\ell' - g_r} \tag{4-33}$$

$$\ell_z'' = \frac{\frac{a_e^2}{\epsilon^2} + \ell' g_z}{\ell' - g_z} \tag{4-34}$$

The above equations can be rearranged as

$$(\ell_r'' - g_r)(\ell' - g_r) = \frac{a_e^2}{\chi^2} + g_r^2 \tag{4-35}$$

$$(\ell_z'' - g_z)(\ell' - g_z) = \frac{a_e^2}{\epsilon^2} + g_z^2 \tag{4-36}$$

These two equations are almost identical in form with a Newtonian lens equation. If the right-hand sides are defined to be f_r^2 and f_z^2, respectively, then the form would match. Thus, the Newtonian lens equations are defined to be

$$(\ell_r'' - g_r)(\ell' - g_r) = f_r^2 \tag{4-37}$$

$$(\ell_z'' - g_z)(\ell' - g_z) = f_z^2 \tag{4-38}$$

with

$$f_r^2 \equiv \frac{a_e^2}{\chi^2} + g_r^2 = \frac{a_e^2}{\chi^2 \sin^2(\chi\phi_e)} \tag{4-39}$$

$$f_z^2 \equiv \frac{a_e^2}{\epsilon^2} + g_z^2 = \frac{a_e^2}{\epsilon^2 \sin^2(\epsilon\phi_e)} \tag{4-40}$$

It must be noted that while f_r and f_z are called the radial and axial focal lengths, they are merely definitions of convenience that permit us to write the lens equations, which are themselves only a convenient form. It is g_r and g_z that are actually important.

I. Post-Electrode Ion Location

The location of an ion is given by y"(x") (4-19) and z"(x") (4-23). It will be convenient later if these two equations are transformed now to simpler forms.

By setting $x'' = \ell_r''$, the ρ_1 coefficient vanishes in equation (4-19), giving us

$$y''(\ell_r'') = a_e \left\{ \frac{\eta}{\chi^2} \left[-\cos(\chi\phi_e) + 1 + \frac{\chi \ell_r''}{a_e} \sin(\chi\phi_e) \right] - \rho_0 \left[\frac{a_e}{\chi \ell'} \sin(\chi\phi_e) + \frac{\ell_r''}{\ell'} \cos(\chi\phi_e) \right] \right\} \tag{4-41}$$

The radial, Newtonian lens equation (4-37) can be rewritten as

$$\ell_r'' = \frac{f_r^2}{\ell' - g_r} + g_r \tag{4-42}$$

By combining the equation for $y''(\ell_r'')$ (4-41) with the equations for ℓ_r'' (4-42), g_r (4-31), and f_r (4-39), we can obtain a new expression for $y''(\ell_r'')$:

$$y''(\ell_r'') = a_e \left\{ \frac{\eta}{\chi^2} \left[1 + \left(\frac{f_r}{\ell' - g_r} \right) \right] - \rho_0 \left(\frac{f_r}{\ell' - g_r} \right) \right\} \tag{4-43}$$

This equation expresses the radial location of an ion in the radial image plane as a function of the ion's relative energy, η, and its radial starting position, ρ_0.

By setting $x'' = \ell_z''$, the ζ_1 coefficient vanishes in equation (4-23), giving us

$$z''(\ell_z'') = -a_e\zeta_0\left[\frac{a_e}{\varepsilon\ell'}\sin(\varepsilon\phi_e) + \frac{\ell_z''}{\ell'}\cos(\varepsilon\phi_e)\right] \tag{4-44}$$

The axial, Newtonian lens equation (4-38) can be rewritten as

$$\ell_z'' = \frac{f_z^2}{\ell' - g_z} + g_z \tag{4-45}$$

By combining the equation for $Z''(\ell_z'')$ (4-44) with the equations for ℓ_z'' (4-45), g_z (4-32), and f_z (4-40), we can obtain a new expression for $z''(\ell_z'')$:

$$Z''(\ell_z'') = -a_e\zeta_0\left(\frac{f_z}{\ell' - g_z}\right) \tag{4-46}$$

This equation expresses the axial location of an ion in the axial image plane as a function of the ion's axial starting position, ζ_0. Note that it is independent of the ion's relative energy, η.

J. Radial and Axial Magnification

Let the entrance slit have a radial width of $w_r' = 2a_e\rho_0$, symmetrically located about $\rho = 0$, i.e., the edges of the slit are located at $\rho = \pm\rho_0$. The width of the image of the entrance slit in the radial image plane is

$$w_r'' = y''(\rho_0) - y''(-\rho_0) \tag{4-47}$$

By equation (4-43), we have

$$w_r'' = a_e \left\{ \frac{\eta}{\chi^2} \left[1 + \left(\frac{f_r}{\ell' - g_r} \right) \right] - \rho_0 \left(\frac{f_r}{\ell' - g_r} \right) \right\}$$
$$-a_e \left\{ \frac{\eta}{\chi^2} \left[1 + \left(\frac{f_r}{\ell' - g_r} \right) \right] + \rho_0 \left(\frac{f_r}{\ell' - g_r} \right) \right\} \qquad (4\text{-}48)$$

or

$$w_r'' = -2a_e\rho_0 \left(\frac{f_r}{\ell' - g_r} \right) = -w_r' \left(\frac{f_r}{\ell' - g_r} \right) \qquad (4\text{-}49)$$

If we define the radial magnification to be $G_r \equiv \left| \frac{w_r''}{w_r'} \right|$, we then have

$$G_r = \left(\frac{f_r}{\ell' - g_r} \right) \qquad (4\text{-}50)$$

Similarly, let the entrance slit have an axial height of $w_z' = 2a_e\zeta_0$, symmetrically located about $\zeta = 0$, i.e., the edges of the slit are located at $\zeta = \pm\zeta_0$. The height of the image of the entrance slit in the axial image plane is

$$w_z'' = Z''(\zeta_0) - Z''(-\zeta_0) \qquad (4\text{-}51)$$

By equation (4-46), we have

$$w_z'' = -a_e\zeta_0 \left(\frac{f_z}{\ell' - g_z} \right) + a_e(-\zeta_0) \left(\frac{f_z}{\ell' - g_z} \right) \qquad (4\text{-}52)$$

or

$$w_z'' = -2a_e\zeta_0 \left(\frac{f_z}{\ell' - g_z} \right) = -w_z' \left(\frac{f_z}{\ell' - g_z} \right) \qquad (4\text{-}53)$$

If we define the axial magnification to be $G_z \equiv \left| \frac{w_z''}{w_z'} \right|$, we then have

$$G_z = \left(\frac{f_z}{\ell' - g_z} \right) \qquad (4\text{-}54)$$

It is now possible to write the post-electrode ion location equations (4-43) and (4-46) in their most compact form. Substituting

the equations (4-50) and (4-54) for G_r and G_z, respectively, into equations (4-43) and (4-46) yields

$$y''(\eta,\rho_0) = a_e\left\{\frac{\eta}{\chi^2}\,[1 + G_r] - \rho_0 G_r\right\} \tag{4-55}$$

$$Z''(\zeta_0) = -a_e\zeta_0 G_z \tag{4-56}$$

It must be noted that, in this section, ρ_0 and ζ_0 are performing double duty. In the derivation of G_r and G_z, ρ_0 and ζ_0 were specific, fixed values. In the two equations above, they are again arbitrary, as per their usual usage.

K. Energy Dispersion

The energy is a measure of how far the image of a beam of ions is displaced because the ion energy is not the energy to which the system is currently tuned. This displacement is called D.

The radial energy dispersion, D_r, and the radial energy dispersion coefficient, K_r, are given by (Ref 4:179), (Ref 5:215), (Ref 6:27)

$$D_r \equiv K_r\eta \tag{4-57}$$

where

$$K_r \equiv \frac{\partial y''}{\partial \eta} \tag{4-58}$$

With the aid of the equation for y" (4-55), we have

$$K_r = \frac{ae}{\chi^2}\;(1 + G_r) \tag{4-59}$$

Similarly, the axial energy dispersion, D_z, and the axial dispersion coefficient, K_z, are given by

$$D_z \equiv K_z\eta \tag{4-60}$$

where $$K_z \equiv \frac{\partial z''}{\partial \eta} \tag{4-61}$$

However, with the help of the equation for z" (4-56), we have

$$K_z = 0 \tag{4-62}$$

Therefore, $$D_z = 0 \tag{4-63}$$

There is no axial energy dispersion, at least not to first order. This is understandable as the major velocity components lie in the radial plane and the axial velocity component is small. One could try to rework the axial equations as a second order approximation, but the axial equation of motion is of a form for which no general method of solution exists. Therefore, it will not be pursued here.

It should be noted that η contains T_0 in the denominator and thus, D_r varies inversely with the mean energy, T_0.

L. Resolution

The absolute resolution is the reciprocal of the minimum difference in absolute energy that can be resolved as two separate lines by the system (Ref 4:179). The relative resolution is the reciprocal of the minimum difference in the relative energy that can be resolved as two separate lines when the system is tuned for the absolute energy, T_0.

The beam image moves inward or outward linearly with η, as η is decreased or increased. This is expressed by the radial dispersion equation

$$D_r = K_r \eta = \frac{ae}{\chi^2} (1 + G_r)\eta \tag{4-57}$$
(4-59)

By inspection of the y" equation (4-55)

$$y''(\eta,\rho_0) = a_e \left| \frac{\eta}{\chi^2} (1 + G_r) - \rho_0 G_r \right| \qquad (4\text{-}55)$$

it can be seen that, for a positive change b_r' in ρ_0, the image moves inward by b_r'', where

$$b_r'' = -b_r G_r \qquad (4\text{-}64)$$

If the entrance and exit slits are symmetrically located about $\rho = 0$, ($y' = y'' = 0$), and have widths w' and w" related by

$$w'' = G_r w' \qquad (4\text{-}65)$$

then a beam of ions of energy $\eta = 0$, with $\rho_0 = 0$ and $\alpha_r' = 0$, will have its image located at $y'' = 0$ (see Figure 10). If the relative energy is increased, the beam image will move outward until it just touches the edge of the exit slit located at $y'' = \frac{w''}{2} = \frac{G_r w'}{2}$. By increasing ρ_0 to $\frac{w'}{2a_e}$, the beam image will move back toward the center of the exit slit. The relative energy can then be increased again until it reaches a value defined as η^+ in which the beam just touches the outer edge of the entrance slit and the beam image just touches the outer edge of the exit slit. The relative energy η^+ is the maximum relative energy a parallel beam of ions into the system can have and still be transmitted through the system.

Similarly, one can decrease the relative energy until the beam image just touches the inner edge of the exit slit located at $y'' = \frac{-w'}{2} = \frac{-G_r w'}{2}$. By decreasing ρ_0 to $\frac{-w'}{2a_e}$, the beam image will move back toward the center of the exit slit. The relative energy can then be decreased further until it reaches a value defined as η^- in which

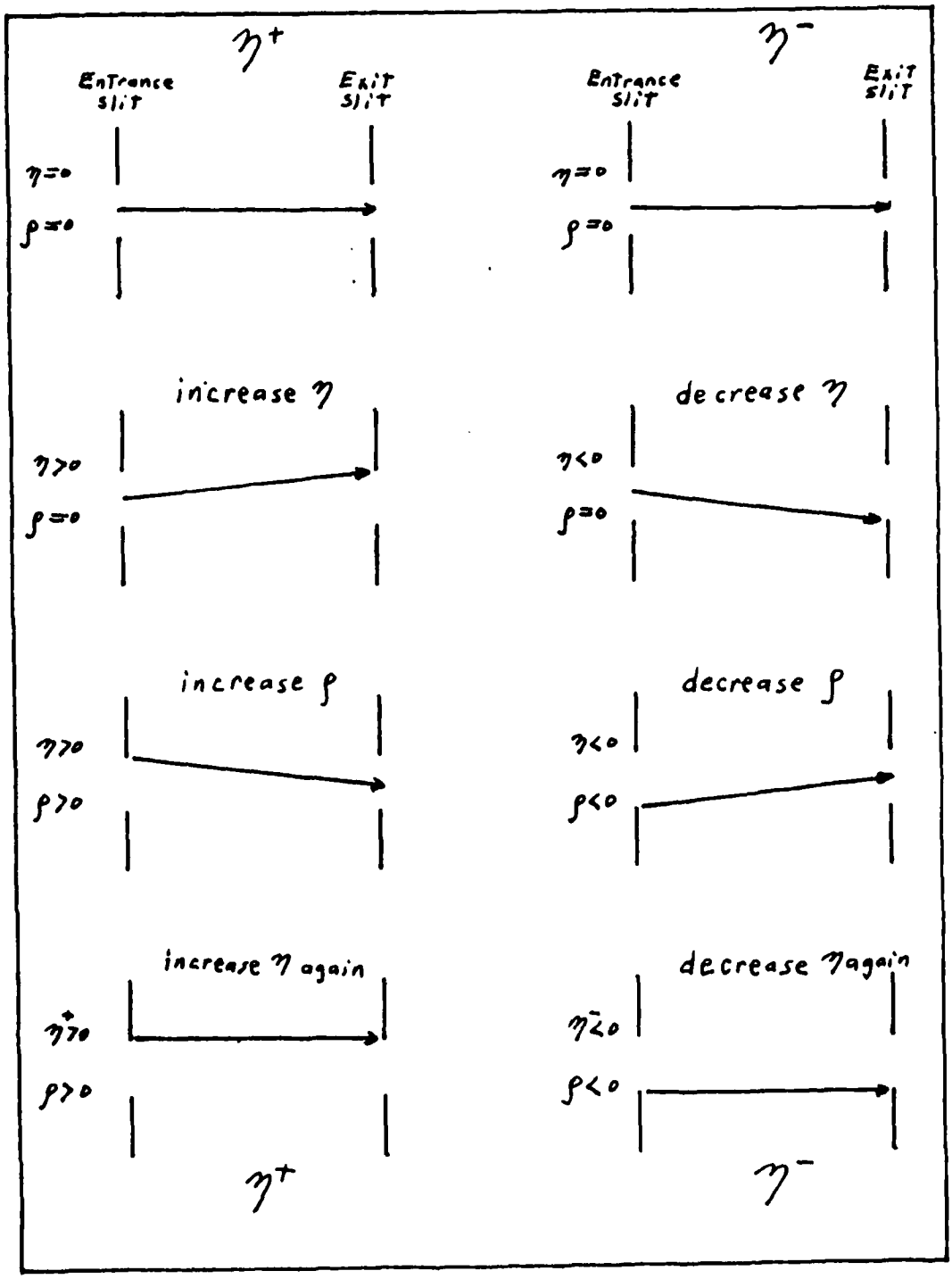

Figure 10 - Graphic Definition of η^+ and η^- the maximum/minimum ion energy transmittable when the system is tuned to $\eta = 0$, $T = T_0$.

the beam just touches the inner edge of the entrance slit and its image just touches the inner edge of the exit slit. The relative energy η^- is the minimum relative energy a parallel beam of ions into the system can have and still be transmitted through the system.

By setting $y'' = \frac{w''}{2} = \frac{G_r w'}{2}$, $\rho_0 = \frac{w'}{2a_e}$, and $\eta = \eta^+$, and inserting these values into the equation for y" (4-55), we get

$$\frac{G_r w'}{2} = a_e \left\{ \frac{\eta^+}{\chi^2} (1 + G_r) - \frac{w'}{2a_e} G_r \right\} \tag{4-66}$$

Solving this equation for η^+ yields

$$\eta^+ = \frac{\chi^2 G_r w'}{a_e(G_r + 1)} \tag{4-67}$$

By setting $y'' = \frac{-w''}{2} = \frac{-G_r w'}{2}$, $\rho_0 = \frac{-w'}{2a_e}$, and $\eta = \eta^-$, and inserting these values into the equation for y" (4-55), we get

$$\frac{-G_r w'}{2} = a_e \left\{ \frac{\eta^-}{\chi^2} (1 + G_r) + \frac{w'}{2a_e} G_r \right\} \tag{4-68}$$

Solving this equation for η^- yields

$$\eta^- = \frac{-\chi^2 G_r w'}{a_e(G_r + 1)} \tag{4-69}$$

The relative resolution is thus

$$\frac{1}{R_{rel}} = \eta^+ - \eta^- = \frac{2\chi^2 G_r w'}{a_e(G_r + 1)} \tag{4-70}$$

or

$$R_{rel} = \frac{a_e}{2\chi^2 w'} \left(1 + \frac{1}{G_r}\right) \tag{4-71}$$

By equation (3-42)

$$\eta = \frac{T - T_0}{T_0} \tag{3-42}$$

Therefore

$$T^+ = T_0\eta^+ + T_0 \tag{4-72}$$

$$T^- = T_0\eta^- + T_0 \tag{4-73}$$

The absolute resolution is thus

$$\frac{1}{R_{abs}} = T^+ - T^- = T_0(\eta^+ - \eta^-) = \frac{T_0}{R_{rel}} \tag{4-74}$$

Therefore

$$R_{abs} = \frac{a_e}{2\chi^2 w' T}\left(1 + \frac{1}{G_r}\right) \tag{4-75}$$

and

$$R_{abs} = \frac{R_{rel}}{T_0} \tag{4-76}$$

That the absolute resolution varies inversely with T_0 is understandable in that, as the energy of the ion beam goes up, it is increasingly difficult to separate the T^+ ions from the T^- ions by the width of the exit slit. This result agrees favorably with Paolini's results (Ref 7:584) once one realizes that Paolini has written the reciprocal of the resolution.

A comparison can be made now between the resolutions of the three curved systems: cylindrical, spherical, and toroidal. For reasons that will be explained in the Applications chapter, G_r will be set equal to one. By taking the appropriate values of Re, we get

Cylindrical: $$R_{rel} = \frac{a_e}{2w'} \tag{4-77}$$

Spherical: $$R_{rel} = \frac{a_e}{w'} \tag{4-78}$$

Toroidal: $$R_{rel} = \frac{a_e}{\chi^2 w'} \tag{4-79}$$

The spherical case has twice the resolution of the cylindrical case. It will be shown in the Applications chapter that, $\chi^2 \geq \frac{1}{4}$. Therefore, the toroidal case has as much as four times the resolution of the spherical case. This is clear motivation for picking the toroidal system over the other systems.

M. Transmission

The transmission, $T(\eta)$, is the fraction of a beam, at a specific energy η, that passes through the exit slit divided by the fraction that passed through the entrance slit. We can ignore ion losses inside the electrodes as we have already assumed that all of the ions remain near the central path. The transmission is thus the fraction overlap of the beam image with the exit slit.

To get the transmission we need to know the location of the edges of the beam image. The edges can be located with the aid of the equation for y" (4-55), keeping in mind that there is an image inversion, that the entrance slit edges are located at $\rho_0 = \pm \frac{w'}{2a_e}$, and $w'' = G_r w'$. The inner edge of the image, y_L'', is given by

$$y_L'' = a_e \left| \frac{\eta}{\chi^2} (1 + G_r) - \frac{w'}{2a_e} G_r \right| \qquad (4\text{-}80)$$

The outer edge of the image, y_U'', is given by

$$y_U'' = a_e \left| \frac{\eta}{\chi^2} (1 + G_r) + \frac{w'}{2a_e} G_r \right| \qquad (4\text{-}81)$$

When $\eta > 0$, y_U'' is outside the area of the exit slit. Thus, the transmission is

$$T(\eta) = \frac{\frac{w''}{2} - y_L''}{w''} \qquad \eta > 0 \qquad (4\text{-}82)$$

or $$T(\eta) = 1 - \frac{a_e}{\chi^2 w'} \left(1 + \frac{1}{G_r}\right) \eta \qquad \eta > 0 \qquad (4\text{-}83)$$

When $\eta > 0$, y_L'' is outside the area of the exit slit. Thus, the transmission is

$$T(\eta) = \frac{y_U'' - \left(-\frac{w''}{2}\right)}{w''} \qquad \eta > 0 \qquad (4\text{-}84)$$

or $$T(\eta) = 1 + \frac{a_e}{\chi^2 w'} \left(1 + \frac{1}{G_r}\right) \eta \qquad \eta > 0 \qquad (4\text{-}85)$$

These two forms can be combined into a single equation that is good for all η, as shown below

$$T(\eta) = 1 - \frac{a_e}{\chi^2 w'} \left(1 + \frac{1}{G_r}\right) |\eta| \qquad (4\text{-}86)$$

Recalling the equation for the relative resolution η (4-71), we can write the transmission in its final form as

$$T(\eta) = 1 - 2 R_{rel} \ |\eta| \qquad (4\text{-}87)$$

A comparison is readily made between the transmissions of the three curved systems. As developed here, all three have transmission curves that have the shape of an isosceles triangle with a peak value of 100%. The difference between the curves is how sharp they are, and that is strictly a function of the resolution. Thus, the toroidal system has the sharpest transmission curve.

N. Summary of Key Optics Equations

For the convenience of the reader, the key optics equations are listed here for future reference.

Radial Entrance Angle, α_r'

$$\alpha_r' = \frac{a_e}{\ell'} (\rho_0 - \rho_1) \tag{4-3}$$

Axial Entrance Angle, α_z'

$$\alpha_z' = \frac{a_e}{\ell'} (\zeta_0 - \zeta_1) \tag{4-4}$$

Radial Exit Angle, α_r''

$$\alpha_r'' = -\chi\left(\rho_1 - \frac{\eta}{\chi^2}\right) \sin(\chi\phi_e) - \alpha_r' \cos(\chi\phi_e) \tag{4-7}$$

Axial Exit Angle, α_z''

$$\alpha_z'' = -\varepsilon\, \zeta_1 \sin(\varepsilon\phi_e) - \alpha_z' \cos(\varepsilon\phi_e) \tag{4-8}$$

Location of Radial Focal Point, g_r

$$g_r = \frac{a_e}{\chi} \cot(\chi\phi_e) \tag{4-31}$$

Location of Axial Focal Point, g_z

$$g_z = \frac{a_e}{\varepsilon} \cot(\varepsilon\phi_e) \tag{4-32}$$

Radial Newtonian Lens Equation

$$(\ell_r'' - g_r)(\ell' - g_r) = f_r^2 \tag{4-37}$$

Axial Newtonian Lens Equation

$$(\ell_z'' - g_z)(\ell' - g_z) = f_z^2 \tag{4-38}$$

Radial "Focal Length", f_r

$$f_r^2 = \frac{a_e^2}{\chi^2} + g_r^2 = \frac{a_e^2}{\chi^2 \sin^2(\chi\phi_e)} \tag{4-39}$$

Axial "Focal Length", f_z

$$f_z^2 = \frac{a_e^2}{\epsilon^2} + g_z^2 = \frac{a_e^2}{\epsilon^2 \sin^2(\epsilon\phi_e)} \tag{4-40}$$

Radial Magnification, G_r

$$G_r = \frac{f_r}{\ell' - g_r} \tag{4-50}$$

Axial Magnification, G_z

$$G_z = \frac{f_z}{\ell' - g_z} \tag{4-54}$$

Radial, Post-Electrode Ion Location ($x'' = \ell_r''$)

$$y''(\eta,\rho_0) = a_e \left| \frac{\eta}{\chi^2} [1 + G_r] - \rho_0 G_r \right| \tag{4-55}$$

Axial, Post-Electrode Ion Location ($x'' = \ell_z''$)

$$z''(\zeta_0) = -a_e \zeta_0 G_z \tag{4-56}$$

Radial Energy Dispersion, D_r

$$D_r = K_r \eta \tag{4-57}$$

Radial Energy Dispersion Coefficient, K_r

$$K_r = \frac{a_e}{\chi^2} (1 + G_r) \tag{4-59}$$

Radial Image Displacement, b_r'' (when entrance slit moved by b_r')

$$b_r'' = -b_r' G_r \tag{4-64}$$

Radial, Relative Energy Resolution, R_{rel}

$$R_{rel} = \frac{a_e}{2\chi^2 w'} \left(1 + \frac{1}{G_r}\right) \tag{4-71}$$

Radial, Absolute Energy Resolution, R_{abs}

$$R_{abs} = \frac{R_{rel}}{T_0} \tag{4-76}$$

Transmission, $T(\eta)$

$$T(\eta) = 1 - 2 R_{rel} |\eta| \tag{4-87}$$

V. Applications

A. Overview

The results from the previous chapters are used in this chapter to work out the behavior of off-center slits. It is the use of off-center slits that gives this analyzer its chief advantage - that of being able to sample different parts of the energy spectra at the same time with a single voltage on the electrodes.

Criteria are developed for minimizing the size of the instrument. This leads to a simplified set of optic equations and lays the foundation for discussing the various trade-offs that must be made in designing an electrostatic analyzer.

Errors in the series solutions are then considered as functions of the deviation from the central path. A discussion is given on how these errors affect the resolution and the transmission. This leads to choosing secondary entrance slits so as to restrict the entry angles so that the ions will remain in regions with no more than a given error in the series solutions to the electric fields.

Finally, a qualitative discussion is given on how to determine the total beam current from what is known about the original ion population. This information is needed in order to make a choice of the entrance slit size when trading-off between the resolution and the detector sensitivity. It is also needed for analyzing the data provided by the instrument.

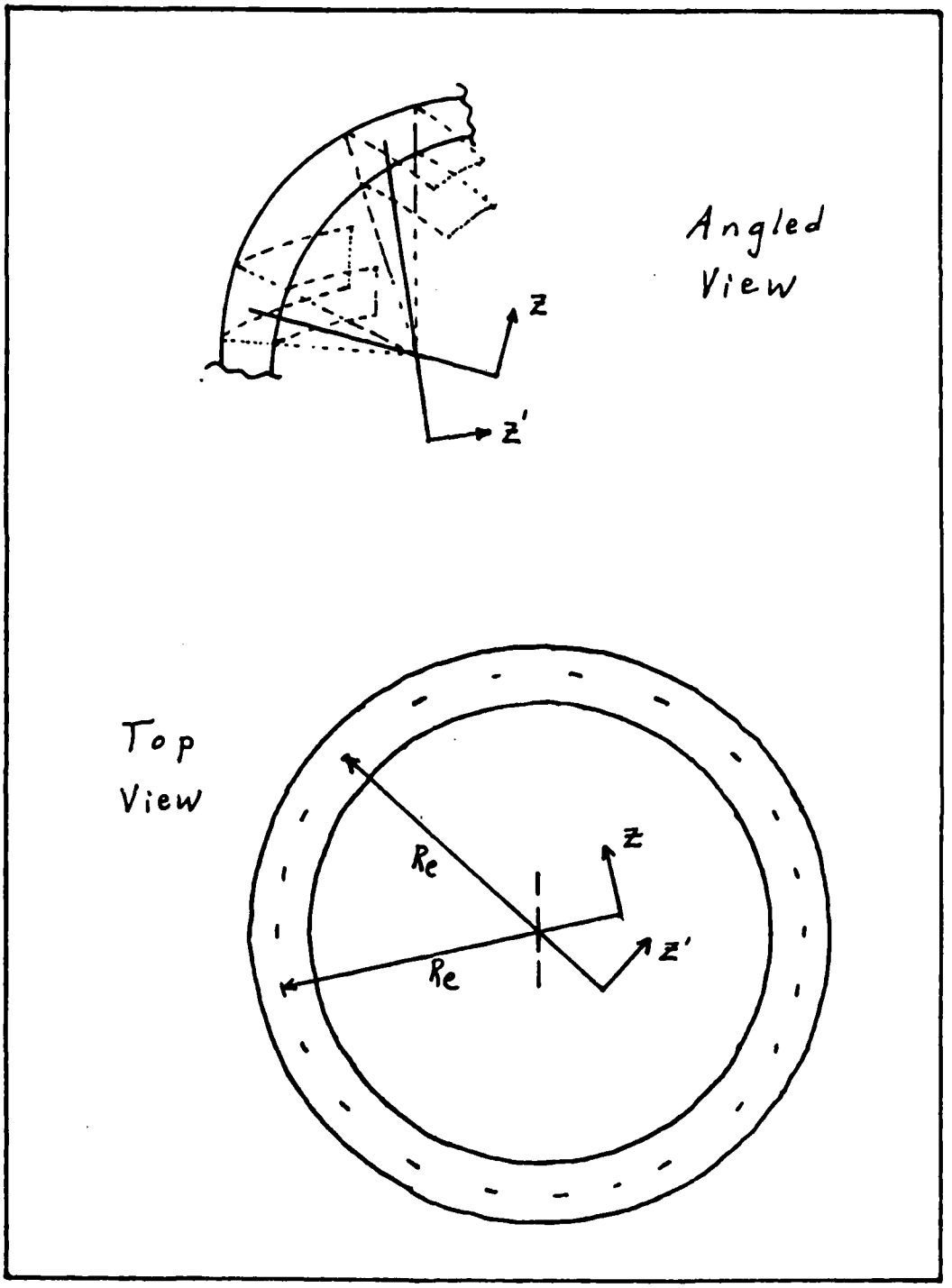

Figure 11 - Rotation of Cylindrical Coordinate System

B. Off-Center Slits

One of the attractions of a toroidal, electrostatic analyzer is that the radii, R_a and R_b, can be allowed to sweep through a full 2π (see Figure 2). This eliminates one pair of edges and their fringe fields. Also, ions can be admitted at any point on the circle, $R = R_e$, and all of the previous results still hold, although a new coordinate system is needed for each new entry point.

These new coordinate systems differ only in that they have been rotated about the center of curvature for R_e (see Figure 11). This rotation yields a new entry point and a new coordinate system, but the equations used for the new coordinate system are identical in form to the original equations used for the original entry point and the original coordinate system.

The advantage of the additional entry points is that their entrance and exit slits can be placed at various off-center locations. This permits the user to sample different mean energies simultaneously. As the voltage on the electrodes is changed, the multiple channels sweep different segments of the energy spectra at the same time. This results in a complete spectra in far less time, which can be critical in experiments with a limited total observation time. A specific example that comes to mind is a pulsed plasma device.

The equation which describes the behavior of off-center slits is

$$y'' = a_e\{\chi^2\eta(1 + G_r) - \rho_0 G_r\} \qquad (4\text{-}55)$$

This can be rewritten as

$$\eta = \left[\frac{1}{\chi^2(1 + G_r)}\right]\left[\frac{y''}{a_e} + \rho_0 G_r\right] \qquad (5\text{-}1)$$

By letting ρ_0 be the center of an off-center entrance slit and y" be the center of the off-center exit slit, equation (5-1) determines the mean, relative energy that is being sampled by that pair of slits.

The voltage that is being applied to the electrodes is hidden inside of η. The relative energy, η, is given by

$$\eta = \frac{T - T_0}{T_0} \tag{3-42}$$

where $T_0 = \frac{1}{2} M_0 v^2$.

From the centripetal force equation (3-9), we have

$$\frac{1}{2} M_0 v_0^2 = \frac{-eE_0 a_e}{2} \tag{3-9}$$

From the electrostatics section, we have

$$E_0 = \frac{2 U_0}{\left\{\frac{a_e}{(\varepsilon^2 - 1)} \ln\left[\frac{(1 + \varepsilon^2\rho_b)(1 - \rho_b)}{(1 - \varepsilon^2\rho_b)(1 + \rho_b)}\right]\right\}} \tag{2-24}$$

where $\rho_b = \frac{d}{2a_e}$ (2-25)

where d is the electrode separation. Therefore, we have

$$T_0 = \frac{-eU_0}{\left\{\frac{1}{(\varepsilon^2 - 1)} \ln\left[\frac{\left(1 + \frac{\varepsilon^2 d}{2a_e}\right)\left(1 - \frac{d}{2a_e}\right)}{\left(1 - \frac{\varepsilon^2 d}{2a_e}\right)\left(1 + \frac{d}{2a_e}\right)}\right]\right\}} \tag{5-2}$$

Equation (5-2) gives the mean, absolute energy, T_0, for which the on-center slits of the analyzer are tuned, in terms of the electrode geometry, the unit charge, and the applied voltage, U_0. It must be

remembered that E_0 is intrinsically negative; therefore, equation (5-2) yields a positive value for T_0.

By combining the equations for T (5-1), T_0 (5-2), and η (3-42), we arrive at

$$T = (\eta + 1)T_0$$

$$= \left\{\left[\frac{1}{\chi^2(1 + G_r)}\right]\left[\frac{y''}{a_e} + \rho_0 G_r\right] + 1\right\}$$

$$* \left\{\frac{-eU_0}{\frac{1}{(\epsilon^2 - 1)} \ln\left[\frac{\left(1 + \frac{\epsilon^2 d}{2a_e}\right)\left(1 - \frac{d}{2a_e}\right)}{\left(1 - \frac{\epsilon^2 d}{2a_e}\right)\left(1 + \frac{d}{2a_e}\right)}\right]}\right\} \qquad (5\text{-}3)$$

This expression gives the mean, absolute energy, T, for an off-center pair of slits, in terms of the location of the entrance and exit slits, the unit charge, the electrode geometry, and the voltage applied to the electrodes.

The range of energies that can be covered, for a fixed voltage, is determined by the available range of values for y" and ρ_0. To avoid ambiguity, for each radial, R, there should be only one entrance slit. The number of exit slits is limited only by the size of the detector behind each slit. The pattern of exit slits can be repeated over and over again, each group with a different entrance slit and thus sampling a different segment of the energy spectrum. The number of groups is limited only by the size of the detectors.

The absolute energy T (5-3) has been plotted as T/eU_0 versus ϵ^2 in the Appendix (see Figures 13, 14, 15), where e is defined to be the

unit charge. In these three figures, I have set the radial magnification to $G_r = 1$; the electrode gap to $d = a_e/50$; and the maximum displacement of the entrance/exit slits to $\frac{y''}{a_e} = \rho_0 = \pm.01$. In Figure 13, the upper energy limit, T_u/eU_0, of the off-center slits is plotted, so we have $\frac{y''}{a_e} = \rho_0 = +.01$. In Figure 14, the lower energy limit, T_ℓ/eU_0, of the off-center slits is plotted, so we have $\frac{y''}{a_e} = \rho_0 = -.01$. In Figure 15, the difference between Figures 13 and 14 has been plotted as $\Delta T/eU_0$. This difference is the maximum range of energies (divided by eU_0) that the system can sample simultaneously at a fixed voltage. For a given value of ϵ^2, the energy, T_0/eU_0, being sampled by the on-center slits is the average of the corresponding values from Figures 13 and 14.

To use these figures: first, choose a value for ϵ^2 and then read $\frac{T_u}{eU_0}$, $\frac{T\ell}{eU_0}$, $\frac{\Delta T}{eU_0}$ off the given curves; second, multiply by a particular value U_0 for the electrode voltage. This will give you T_u, T_ℓ, and ΔT in terms of ev. T_0, in ev, is the average of T_u and T_ℓ.

To illustrate this let us pick $\epsilon^2 = 1.94$. We then have (in ev), $T_u = 58U_0$, $T_\ell = 42U_0$, and $\Delta T = 16U_0$. For $U_0 = 160$ volts, we then get $T_u = 9.28$ kev, $T_0 = 8.0$ kev, $T_\ell = 6.72$ kev. ΔT is 2.56 kev, or about 32% of T_0.

By comparison, for a cylindrical system, we have $\epsilon^2 = 0$. Therefore, in ev, $T_u = 50.2U_0$, $T_\ell = 49.7U_0$, and $\Delta T = .5U_0$. ΔT is about 1% of T_0. For a spherical system, $\epsilon^2 = 1$. Therefore, in ev, we have $T_u = 50.5U_0$, $T_\ell = 49.5U_0$, and $\Delta T = U_0$. ΔT is about 2% of T_0. For a toroidal system, the optimum value of ϵ^2 is 1.94 (this is discussed later in this chapter). This gives us, in ev, $T_u = 58U_0$, $T_\ell = 42U_0$, and $\Delta T = 16U_0$. ΔT is

about 32% of T_0. The toroidal system clearly has the advantage over the other two systems.

The energy range sampled, ΔT, grows as $|\varepsilon^2| \to 2$. By good fortune, the resolution also is maximized by $|\varepsilon^2| \to 2$ (to be shown later). It is the improvement in the energy range and resolution that makes the toroidal system more attractive than the spherical system.

A discrete sampling of the energy spectra can be obtained by driving the applied voltage with a staircase waveform. If the steps have a slight ramp shape, then a continuous spectra can be obtained while the jumps prevent unnecessary overlap.

Due to the linearity of the equations involved, the resolution of an off-center pair of slits is the same as it is for the on-center slits, and is given by

$$R_{rel} = \frac{a_e}{2\chi^2 w'} \left(1 + \frac{1}{G_r}\right) \qquad (4\text{-}71)$$

The transmission curve is unchanged in shape, but it is shifted in the relative energy. If η' is the relative energy for which the off-center pair of slits is tuned, as per equation (5-1), then the transmission is given by

$$T(\eta) = 1 - 2 R_{rel} (|\eta| - \eta') \qquad (5\text{-}4)$$

C. Instrument Size-Maximum Compactness

If one neglects the size of the instrument for a moment and tries instead to maximize the resolution, one quickly discovers that no physically realizable maximum exists with respect to the parameters a_e and R_e. A maximum does exist for the parameter ϕ_e in a form which requires $\chi = 0$; therefore, $\chi\phi_e = 0$, which forces the slits outwards to

infinity. If ℓ', the object distance, is set to $\ell' = K^* g_r$, a multiple of the distance to the focal point, the problem remains for the parameters a_e and R_e, while the maximum with respect to ϕ_e now requires $\chi\phi_e = n\pi$, $n = 0,2,4 \ldots$. Unfortunately, this choice of $\chi\phi_e$ requires that the entrance and exit slits be located at infinity.

The above discussion immediately brings home the need to hold down on the size of the instrument, especially the separation of the two slits. The Newtonian lens equation gives us

$$(\ell_r'' - g_r)(\ell' - g_r) = f_r^2 \qquad (4\text{-}37)$$

It can be shown with elementary calculus that if the product AB = constant, then the sum, A + B, is a minimum if A = B. This gives us the requirement

$$\ell_r'' = \ell' \qquad (5\text{-}5)$$

Therefore, equation (4-37) becomes

$$(\ell' - g_r)^2 = f_r^2 \qquad (5\text{-}6)$$

It is obvious that ℓ' is a minimum if

$$g_r = 0 \qquad (5\text{-}7)$$

At first thought, it would seem that having the focal point located at zero is unreasonable, but it must be remembered that this is not a thin system. It is entirely possible to have the focus located at zero. Having the focal point located at zero means that it is located in the plane that contains the exit end of the electrodes.

By equation (4-31), we have

$$g_r = \frac{a_e}{\chi} \cot(\chi\phi_e) \tag{4-31}$$

$g_r = 0$, implies that

$$\chi\phi_e = \frac{\pi}{2} \tag{5-8}$$

We could set $\chi\phi_e$ equal to higher, odd multiples of $\frac{\pi}{2}$, but we must have ϕ_e less than 2π and this would require that χ increase. Unfortunately, increasing χ decreases the resolution. Thus, the best resolution is maintained by discarding the higher, odd multiples of $\frac{\pi}{2}$. Therefore, the best compactness can be accomplished by requiring that $\ell_r'' = \ell'$ and $\chi\phi_e = \frac{\pi}{2}$.

D. Simplified Optic Equations

The requirements imposed by equations (5-5) and (5-8) (from the previous section) give us the following simplified optic equations:

$$\phi_e = \frac{\pi}{2\chi} \qquad \left(\chi^2 = |2 - \epsilon^2|\right) \qquad \left(\epsilon^2 = \frac{a_e}{R_e}\right) \tag{5-9}$$

$$g_r = 0 \tag{5-10}$$

$$g_z = \frac{a_e}{\epsilon} \cot\left(\frac{\pi\epsilon}{2\chi}\right) \tag{5-11}$$

$$\ell' = \ell_r'' = f_r = \frac{a_e}{\chi} \tag{5-12}$$

$$\ell_z'' = \frac{f_z^2}{\frac{a_e}{\chi} - g_z} + g_z \tag{5-13}$$

$$f_z = \frac{a_e}{\epsilon \sin\left(\frac{\pi\epsilon}{2\chi}\right)} \tag{5-14}$$

$$G_r = 1 \tag{5-15}$$

$$G_z = \frac{f_z}{\frac{a_e}{\chi} - g_z} \tag{5-16}$$

$$R_{rel} = \frac{a_e}{\chi^2 w'} \tag{5-17}$$

$$T(\eta) = 1 = \frac{2a_e}{\chi^2 w'} \quad (|\eta| - \eta') \tag{5-18}$$

(for on-center slits $\eta' = 0$)

The last two equations can be further simplified if we set $w' = Ka_e$. Typically, K has values on the order of 10^{-2}. This gives us

$$R_{rel} = \frac{1}{K\chi^2} \tag{5-19}$$

$$T(\eta) = 1 - \frac{2}{K\chi^2} (|\eta| - \eta') \tag{5-20}$$

These simplified equations are graphically represented in the Appendix. In several cases, the equation has been divided by a_e before plotting so as to get a curve of greater utility. The curves have been plotted with the restriction that $\phi_e < 2\pi$ and most of them have a common ε^2 horizontal axis. These curves should make it easier for the reader to select parameters for his own instrument.

E. Trade-offs and Constraints

The selectable parameters are a_e, R_e, ϕ_e, K (the slit width), and d (the electrode gap). These parameters determine ℓ', ℓ_r'' (the slit locations), R_{rel} (the resolution), and strongly affect the voltage supply requirements, the ion beam current, and thus, the detector sensitivity requirements. Any constraints which are imposed on these additional parameters strongly impact on the allowable values of the

selectable parameters a_e, R_e, ϕ_e, K, and d. Some guidelines can be worked out in advance without knowledge of any specific application.

The resolution goes to infinity as χ^2 approaches zero, or as ϵ^2 approaches two. We are restricted, however, to values of ϵ^2 such that

$$\chi = \sqrt{|2 - \epsilon^2|} \geq \frac{1}{4} \tag{5-21}$$

Values of $\chi < \frac{1}{4}$., force $\phi_e > 2\pi$, which is physically impossible. Also, as χ approaches zero, the slits move out toward infinity and we again have a size problem.

An examination of the curve for ℓ_z''/a_e (see Figure 20), shows the existence of several poles. Advantage can be taken of the poles by picking a value of ϵ^2 close to the pole such that $\ell_z'' = \ell_r''$. This would make the radial and axial image planes coplanar. Perhaps the best reason for doing this is to hold down axial extent of the ion beam in the radial image plane. This is not essential but would help to avoid unwanted losses at the axial ends of the exit slit, which must be located in the radial image plane. It also helps to keep the beam intensity up and to hold down on the axial size of the detector, permitting more groups of detectors to be used.

A numerical search of the region between $\epsilon^2 = 2 - \frac{1}{16}$ and the first pole to the left yields

$$\epsilon^2 \simeq 1.897 \tag{5-22}$$

$$\frac{\ell_z''}{a_e} = \frac{\ell_r''}{a_e} = \frac{\ell'}{a_e} = 3.116 \tag{5-23}$$

$$K^* R_{rel} = 9.708 \tag{5-24}$$

A numerical search of the region between $\epsilon^2 = 2 + \frac{1}{16}$ and the first pole to the right yields

$$\epsilon^2 = 2.115 \tag{5-25}$$

$$\frac{\ell_z''}{a_e} = \frac{\ell_r''}{a_e} = \frac{\ell'}{a_e} = 2.951 \tag{5-26}$$

$$K^* R_{rel} = 8.708 \tag{5-27}$$

The first value for ϵ^2 [equation (5-22)] has a higher resolution than the second value for ϵ^2 [equation (5-25)]. This is at the expense of having the slits farther away, which requires a larger instrument. It should be remembered that these values only pin down $\epsilon^2 = \frac{a_e}{R_e}$, and not the actual values of a_e and R_e.

It is the size constraints that heavily influence the choice of a_e and R_e. This breaks down into two major considerations: first, how much room is available for the electrodes; second, where do the slits have to be with respect to the electrodes. If one accepts the constraint imposed earlier that $\ell_z'' = \ell_r''$ and if the size of the electrodes is the primary concern, then one would pick R_e, and calculate a_e from ϵ^2 in equations (5-22) or (5-25). If the location of the slits is the primary concern, then one would use equations (5-23) or (5-26) to determine a_e, and then R_e would be calculated from equations (5-22) or (5-25).

A complication in choosing a_e and R_e is that the outer electrode has an actual size of $r_b = a_e + \frac{d}{2}$ and $R_b = R_e + \frac{d}{2}$, where d is the electrode gap. The choice of d directly affects the voltage that must be applied to the electrodes to get a given value of E_0, the

central path electric field strength, via equation (2-24). This impacts on the voltage supply requirements.

A further complication is that with a_e and R_e chosen (and thus ϵ^2), one must now pick K to get the resolution desired via equation (5-19). As K gets smaller, the ion current goes down and this impacts on the detector sensitivity required. The detector sensitivity is further affected by the strength of the ion source that will be presented to the analyzer entrance slit.

The choices are not easy and will probably require many trials before an acceptable compromise is reached. Hopefully, the curves in the Appendix will speed up the initial selection process.

F. Ion Path vs Field Error

It was initially assumed that all ions would have trajectories near the central path and that the electric field could be given by equations (2-34) and (2-35). However, as the ions radially deviate from the central path, the error grows in the series approximation to the radial field. By comparing the series solution to the exact solution assumed by H. Wollnik (Ref 4:166) [equation (2-20)], it is possible to estimate the percent error in the series solution as a function of ρ, the deviation from the central path. The percent error is defined as

$$\% \text{ radial error} = \frac{E_r(\rho) - E_{Wollnik}(\rho)}{E_{Wollnik}(\rho)} * 100 \qquad (5\text{-}28)$$

with $\zeta = 0$.

This equation has been plotted in the Appendix (see Figure 26). It should be noted that the curve shows that the percent error grows

more rapidly for positive ρ than it does for negative ρ. In both cases, the series solution underestimates the strength of the radial field.

Starting from an on-center slit, the underestimation of the radial field is going to result in the ion pattern being shifted toward lower values of ρ. The pattern is fixed at $\rho = 0$ because the percent error is zero for $\rho = 0$. Lower energy ions that traverse the $\rho < 0$ region will be transmitted in lower numbers than expected. Contrawise, the higher energy ions which traverse the $\rho > 0$ region will be transmitted in higher numbers than expected. In fact, due to the greater error when $\rho > 0$, more high energy ions will be picked up than low energy ions are lost. This will shift and distort the transmission curve. Also, the resolution will be slightly less sharp than expected because of the field errors.

The axial field series solution usually overestimates the true field strength, but the percent error is symmetric about $\zeta = 0$, and has no effect on the resolution.

If one considers Figure 12, one can see that the percent error in the axial field is given by

$$\% \text{ axial error} = \frac{E_z(\zeta) - \sin\theta E_{\text{Wollnik}}(\rho^*)}{\sin\theta E_{\text{Wollnik}}(\rho^*)} * 100 \qquad (5\text{-}29)$$

where

$$\rho^* = \frac{1}{\epsilon^2}\left(\sqrt{(1 + \epsilon^2\rho)^2 + (\epsilon^2\zeta)^2} - 1\right) \qquad (5\text{-}30)$$

The overestimation of the axial means that fewer ions will be focused back onto the slit. As this effect is weaker for $\rho > 0$, the high energy ions will have their transmission reduced less than the

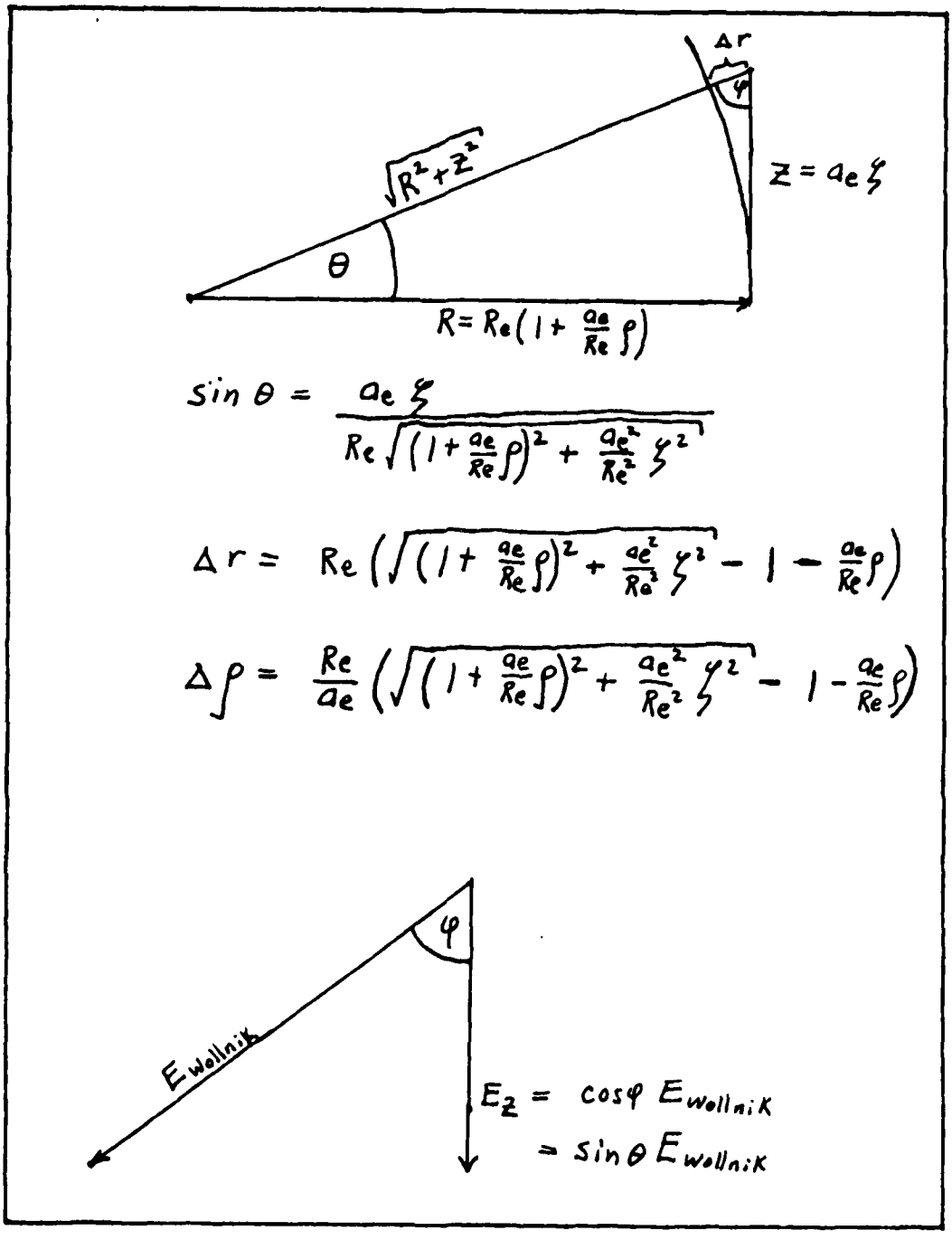

Figure 12 - Axial Component of Exact Electric Field

lower energy ions. This increases the distortion in the transmission curve caused by the radial field errors. However, it does nothing to the resolution.

A rough estimate of the axial field errors can also be gained by the use of equation (2-8). This equation gives the equipotential curves in the half plane (ϕ = constant) as curves of $\rho = f(\zeta)$. This has been plotted with ε^2 set equal to two (see Figure 27). Included in the graph is an equipotential curve through $\rho = 0$ and $\zeta = 0$, as envisioned by H. Wollnik (Ref 4:166). Note that the error is symmetric about $\zeta = 0$.

As the off-center slits are more likely to direct their ions through regions away from the central path, their resolution and transmission curves are more likely to suffer distortion and degradation due to the field errors than are the on-center slits.

G. Entrance Angles versus Field Errors

If one picks a maximum percent error that will be tolerated in the radial electric field, then, with the help of Figure 18 in the Appendix, a value for the maximum permissible ρ can be chosen. The question remains: what is the maximum permissible radial entrance angle, α_r', such that $\rho \leq \rho_{max}$ for all ϕ? To get an answer, we need the solution to the radial equation of motion:

$$\rho(\phi) = \left(\rho_1 - \frac{\eta}{\chi^2}\right) \cos(\chi\phi) - \frac{\alpha_r'}{\chi} \sin(\chi\phi) + \frac{\eta}{\chi^2} \qquad (3\text{-}44)$$

By equation (4-3), we have

$$\alpha_r' = \frac{ae}{\ell T} (\rho_0 - \rho_1) \qquad (4\text{-}3)$$

or

$$\rho_1 = \rho_0 - \frac{\alpha_r' \ell'}{a_e} \tag{5-31}$$

Therefore,

$$\rho(\phi) = \left(\rho_0 - \frac{\alpha_r' \ell'}{a_e} - \frac{\eta}{\chi^2}\right) \cos(\chi\phi) - \frac{\alpha_r'}{\chi} \sin(\chi\phi) + \frac{\eta}{\chi^2} \tag{5-32}$$

The geometry of the instrument will pin down ℓ', a_e, and χ. ρ_0 can be set equal to the radial center of the entrance slit of interest, and η can be calculated from equation (5-1) for the pair of slits being considered. Rho is constrained by $\rho \leq \rho_{max}$, as selected from Figure 18 in the Appendix. A computer search can now be made, with ϕ as the independent variable, to find the value of α_r' that yields $\rho \leq \rho_{max}$. Due to the asymmetry of Figure 18, there exists two values for α_r': one for ions that leave the entrance slit heading outwards ($\rho > 0$), and one for ions heading inwards ($\rho < 0$).

By adding a secondary entrance slit behind the primary entrance slit, ions with too large of a radial entrance angle can be eliminated. The edges of the secondary slit are situated so as to be consistent with the two values of α_r' just computed. This will ensure that the ions are constrained to the region surrounding the central path with a percent field error less than or equal to the maximum error that one has chosen to tolerate.

A similar calculation can be done for the axial entry angle, α_z'. The solution to the axial equation of motion is

$$\zeta(\phi) = \zeta_1 \cos(\varepsilon\phi) - \frac{\alpha_z'}{\varepsilon} \sin(\varepsilon\phi) \tag{3-51}$$

where

$$\alpha_z' = \frac{a_e}{\ell'} (\zeta_0 - \zeta_1) \qquad (4\text{-}4)$$

or

$$\zeta_1 = \zeta_0 - \frac{\alpha_z' \ell'}{a_e} \qquad (5\text{-}33)$$

Therefore,

$$\zeta(\phi) = \left(\zeta_0 - \frac{\alpha_z' \ell'}{a_e}\right) \cos(\varepsilon\phi) - \frac{\alpha_z'}{\varepsilon} \sin(\varepsilon\phi) \qquad (5\text{-}34)$$

The geometry of the instrument will pin down ℓ', a_e, and ε. ζ_0 can be set to the axial center of the entrance slit, $\zeta_0 = 0$. Zeta is constrained by $\zeta \leq \zeta_{max}$, where ζ_{max} is obtained from equation (5-29). A computer search can now be made, with ϕ as the independent variable, to find the value of α_z' that yields $\zeta \leq \zeta_{max}$. Due to the symmetry involved, only one value of α_z' exists.

The entrance slit is relatively narrow in the radial direction, and the radial entrance angle permitted by the primary and secondary slits does not vary too much from α_r' (max) for ions that enter near the radial edge of the slit. However, the entrance slit is relatively long in the axial direction. To hold down on the deviation of the maximum permissible, axial entry angle from α_z' (max), the axial secondary slit edges need to be far away from the primary slit, i.e., as close to the electrodes as possible. This can be accomplished with a single secondary slit located near the electrodes with both the appropriate axial and radial edges.

The existence of the secondary slit accomplishes four things: first, it limits ion trajectories to the central region; second, it

prevents ions from straying from one group of exit slits to another group causing an ambiguity in the data; third, it defines the soli angle of acceptance of the primary entrance slit; and fourth, it serves to hold down on the fringe fields. It might also be desirable to place a matching secondary slit on the exit end of the electrodes.

H. Total Beam Current

The total beam current must be arrived at with statistical mechanics. The procedure will be qualitatively outlined below. No exact equations will be given since the problem is too dependent on the particular experiment for any one set of equations to be of much use. There are four statistical populations that must be worked out in order to get the beam current.

The first population is the ionized plasma that is under observation. This part of the problem is solely a function of the experiment being conducted.

The second population is the plasma that comes through the primary slit. This part of the problem is essentially that of a gas escaping through a small hole in a container with an unlimited supply of gas in the container. One must also take into account whether or not there is a net motion of the plasma relative to the primary entrance slit. If the plasma is dense or hot, as in a pulsed plasma device, then plasma effects such as magnetohydrodynamics may have to be considered. In general, the second population will have a higher average energy than the first population. It will also have an angular distribution that is peaked in the forward direction.

The third population is that portion of the second population that clears the secondary slit. It can be determined by integrating

the second population over the solid angle defined by the primary and secondary slits.

The fourth population is that portion of the third population that clears the exit slit. It can be determined by multiplying the third population's distribution function by the transmission function and then integrating over energy. The result of the integration is the total beam current as seen by the detector.

If the primary slit width and length have been carried along as unspecified parameters, then we will now have the beam current as a function of the slit's width and length. It will now be possible to make the trade-off between detector sensitivity and the resolution by selecting the appropriate slit width and length.

The only problem with all of this is that, if the first population's distribution function were known, then we would not need the analyzer at all. If an approximate model is available, the above procedure can be used to select the primary slit. In general, one needs to start with the detector and work backwards so as to connect the detector data to the original population. This can be made simpler if one assumes that the original population obeys Maxwell-Boltzmann statistics. It is still essential to know how the plasma is moving with respect to the primary slit.

One fact that simplifies things is that the resolution and transmission are in terms of the ion kinetic energy, T, outside the field and the kinetic energy, T_0, of an ion that obeys the centripetal force equation. This gets one outside of the electrodes but inside the secondary entrance slit. The secondary entrance slit only clips the angular distribution and does not really affect the energy

spectra. Thus, the detector data can be directly related to the number of ions passing through the primary slit with a specific energy.

I. Conclusion

A toroidal geometry, electrostatic analyzer has several distinct advantages: first, it can be used as a multi-channel analyzer sampling different segments of the energy spectra at the same time; second, the range of energies that can be sampled simultaneously is more than an order of magnitude wider than it is with either a cylindrical or a spherical system; and third, the resolution is significantly higher than it is with either a cylindrical or a spherical system. These advantages definitely enhance the speed and accuracy of the electrostatic analyzer.

J. Recommendations

My recommendations are twofold. First, the fringe fields need to be treated more accurately. Perhaps Albrecht's work (Ref:3) will be of some help. Second, the image aberrations need further studying. This will necessitate an investigation of higher order terms in the electrostatic equations, the mechanic equations, and the optic equations.

Bibliography

1. Svartholm, N. "Velocity and Two-Directional Focusing of Charged Particles in Crossed Electric and Magnetic Fields, I," ARKIV FÖR FYSIK, Band 2 nr 20:195-207 (1950).

2. Ewald, H. and Liebl, H. "Der Astigmatismus der Toroid-Kondensators," Z. Naturforsch, 10a:872-876 (1955).

3. Albrecht, R. "Das Potential in doppelt geKrümmten Kondensatoren," Z . Naturforsch, 11a:156-163 (1956).

4. Wollnik, H. "Electrostatic Prisms," Focusing of Charged Particles, Volume 2, edited by A. Septier. New York: Academic Press, 1967.

5. Duckworth, H. E. and Ghoshal, S. N. "High-Resolution Mass Spectroscopes," Mass Spectrometry, edited by C. A. McDowell. New York: McGraw Hill Book Company, Inc., 1967.

6. Dahl, P. Introduction to Electron and Ion Optics, New York: Academic Press, 1973.

7. Paolini, F. R. and Theodoridis, G. C. "Charged Particle Transmission through Spherical Plate Electrostatic Analyzers," The Review of Scientific Instruments, 38:579-588 (May, 1967).

Appendix

Representative Design Curves

Shown on the following pages are graphs which should help the reader to design his own instrument. Most of these curves have been plotted with a common ϵ^2-axis, where ϵ^2 is the ratio of the two radii, $\frac{a_e}{R_e}$, of the mid-electrode surface. It should be noted that several of the curves have been divided by a_e, to get curves that are of greater utility.

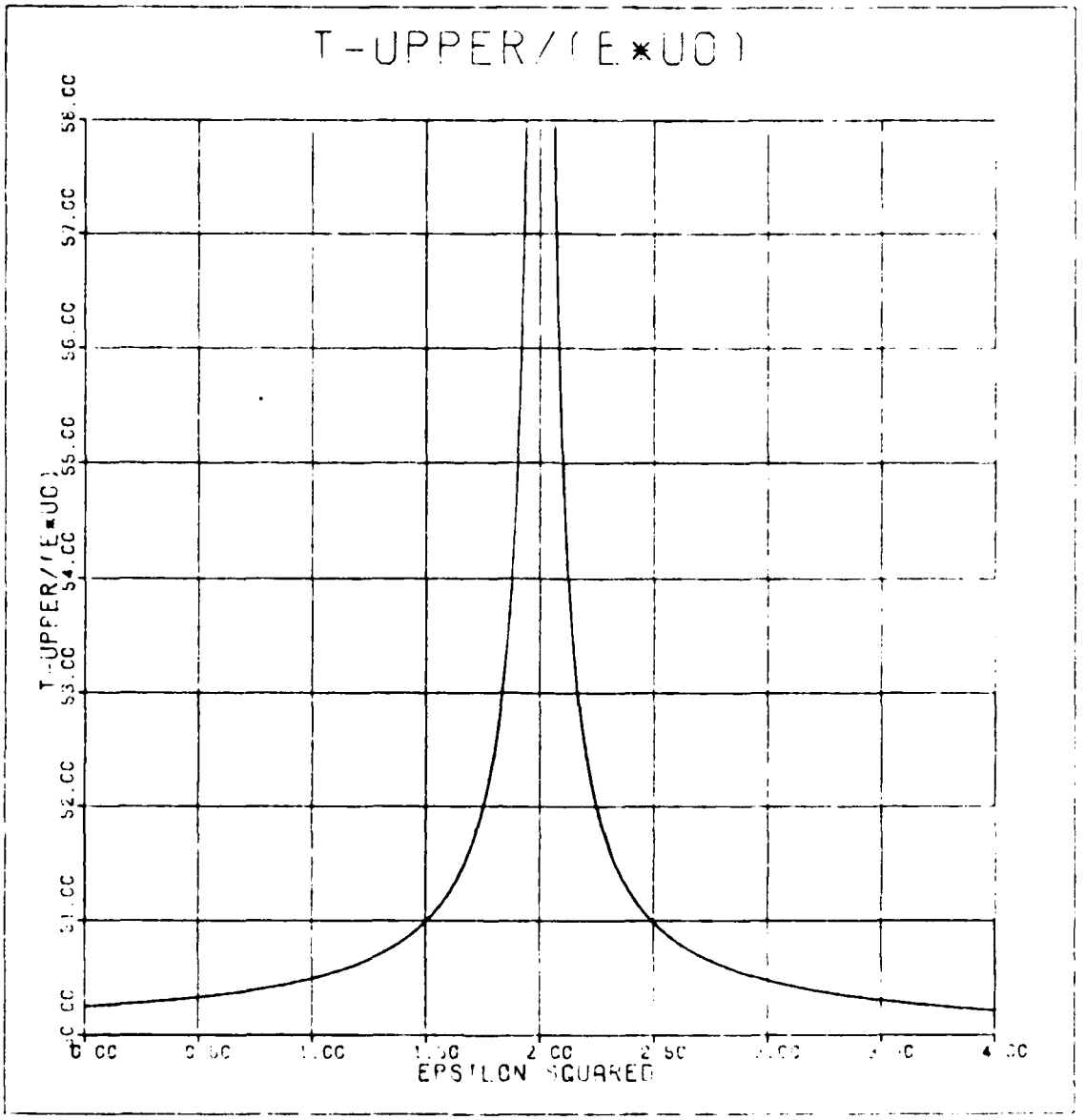

Figure 13 - Upper Energy Limit of Off-Center Slits

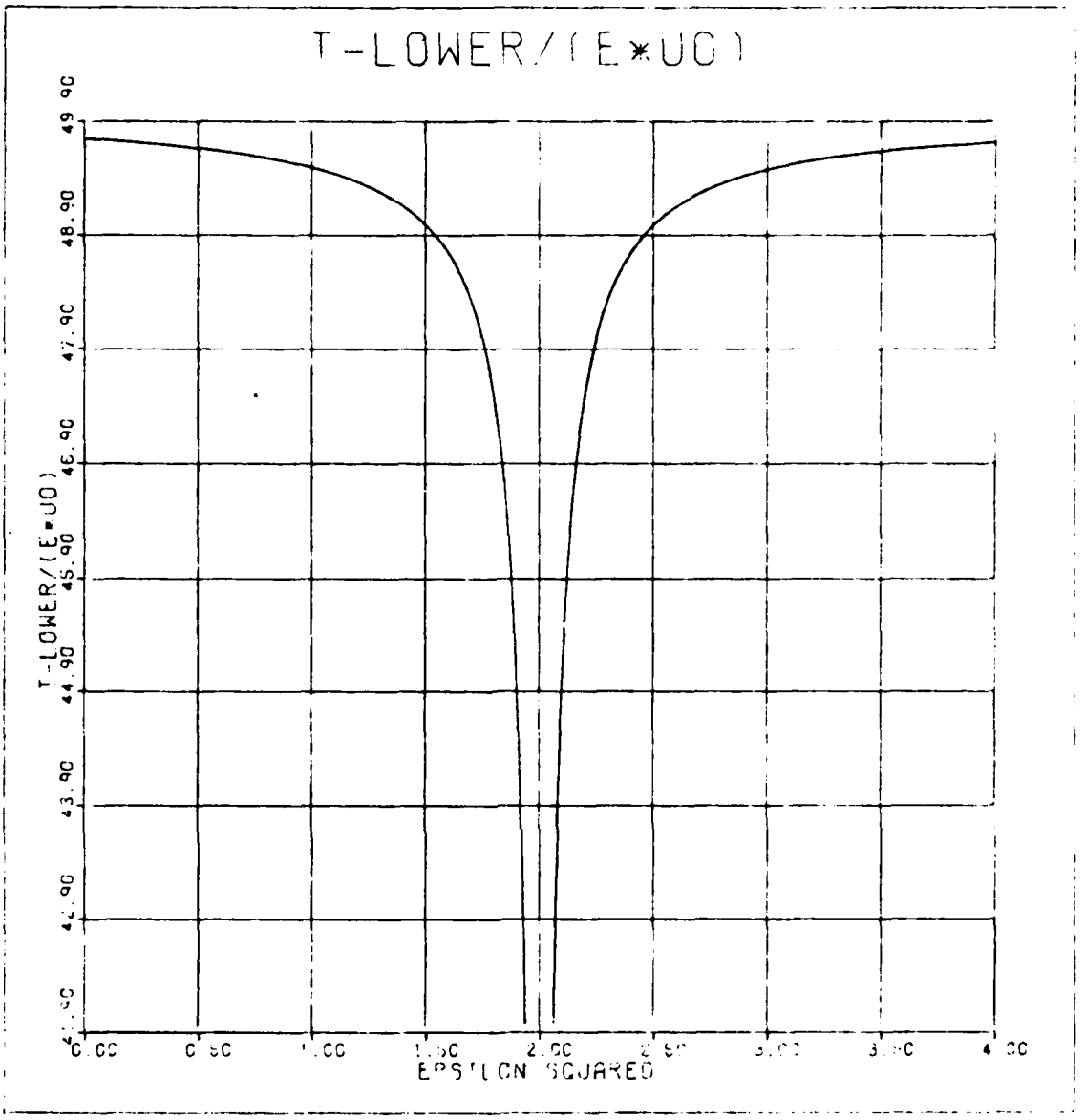

Figure 14 - Lower Energy Limit of Off-Center Slits

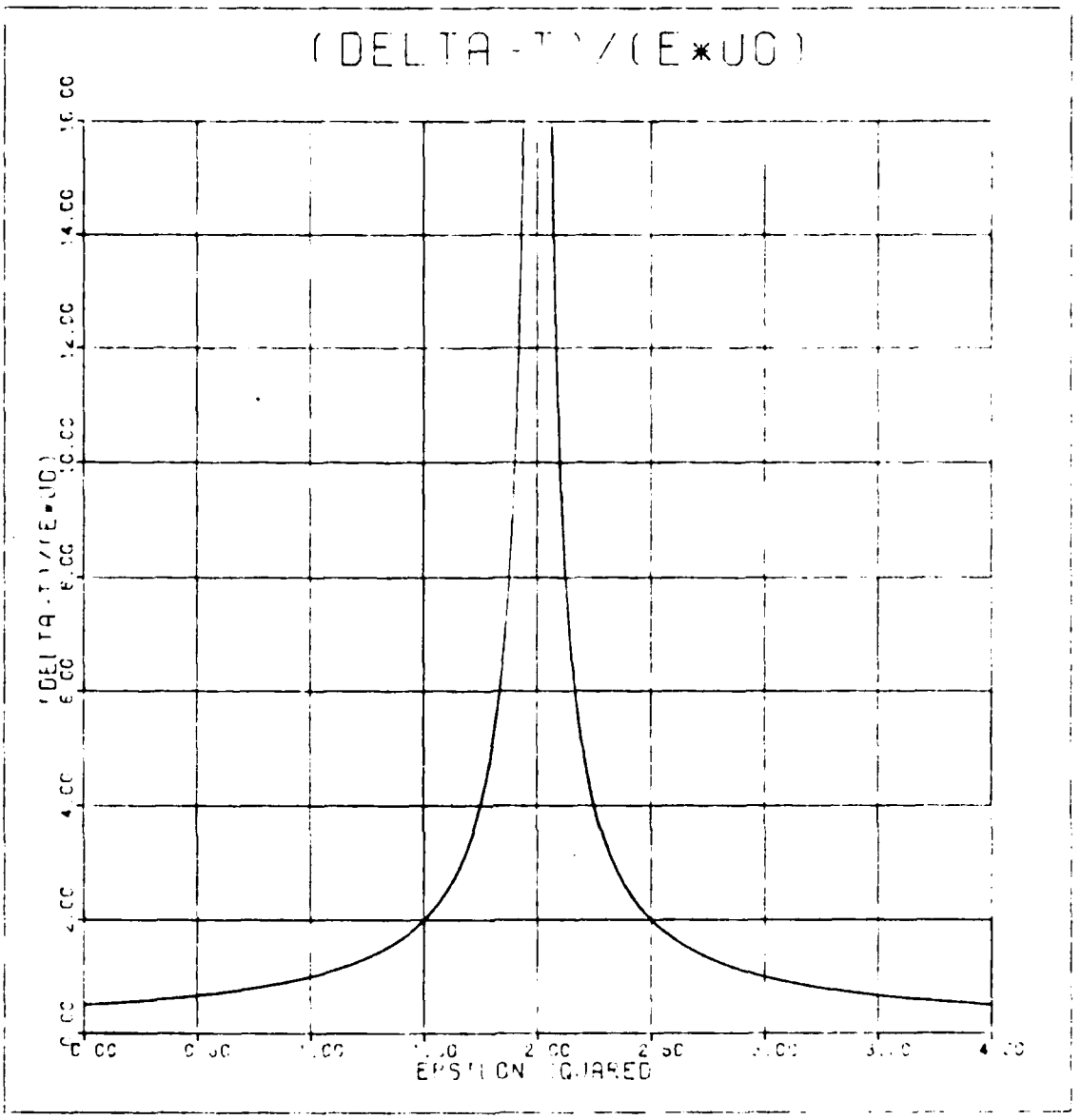

Figure 15 - Energy Range of Off-Center Slits

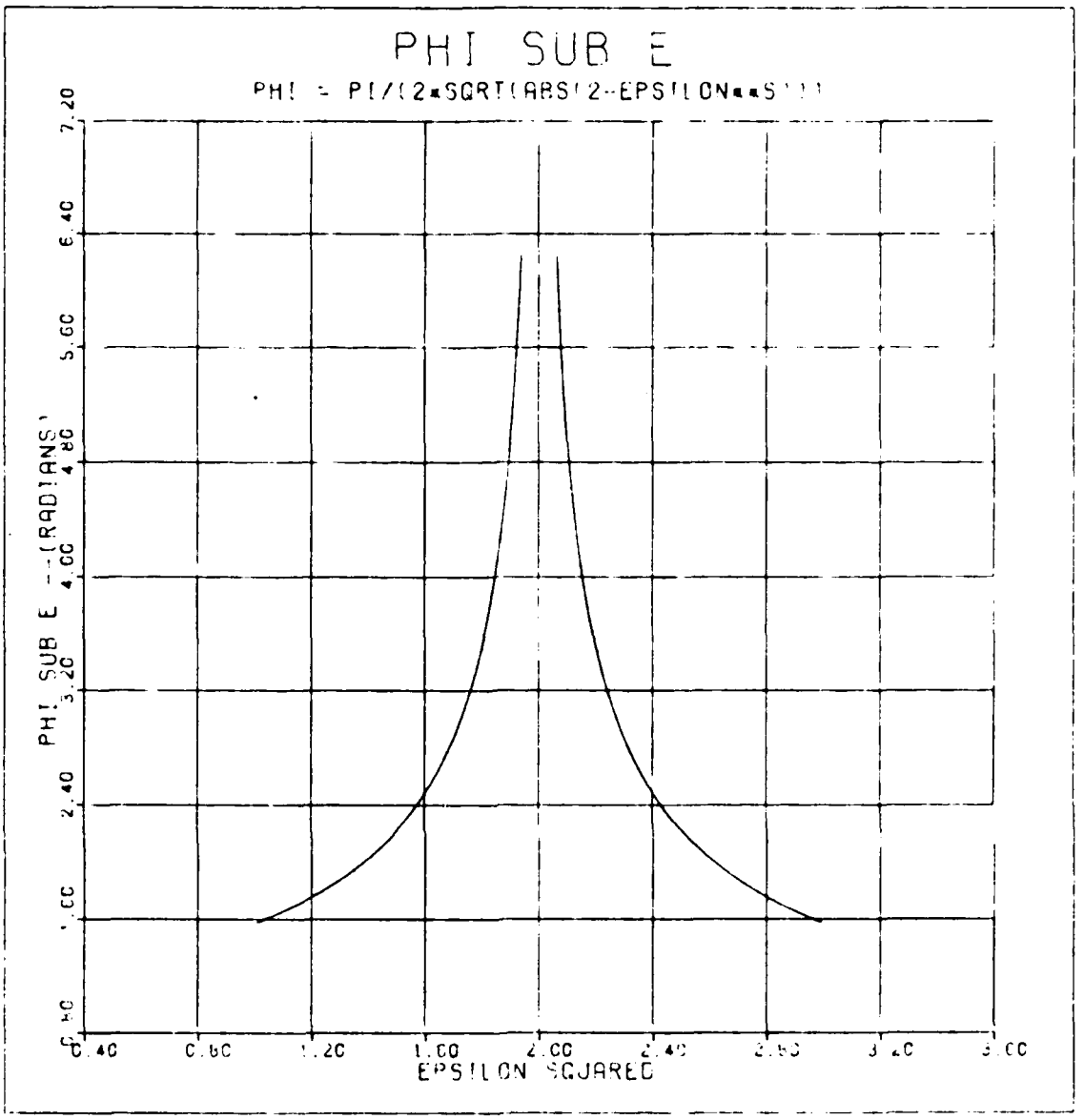

Figure 16 - Angular Extent of Electrodes

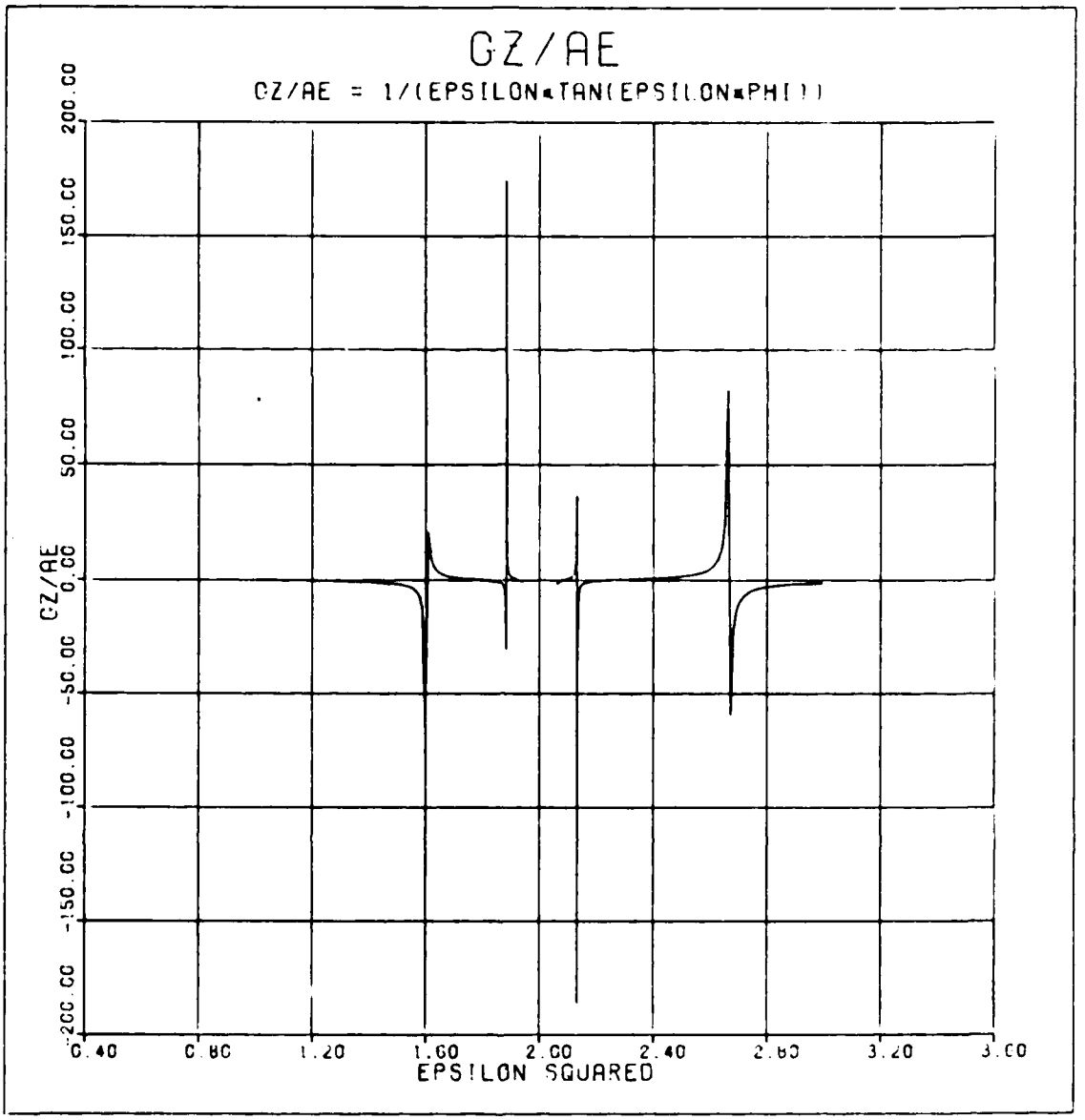

Figure 17 - Location of Axial Focal Point

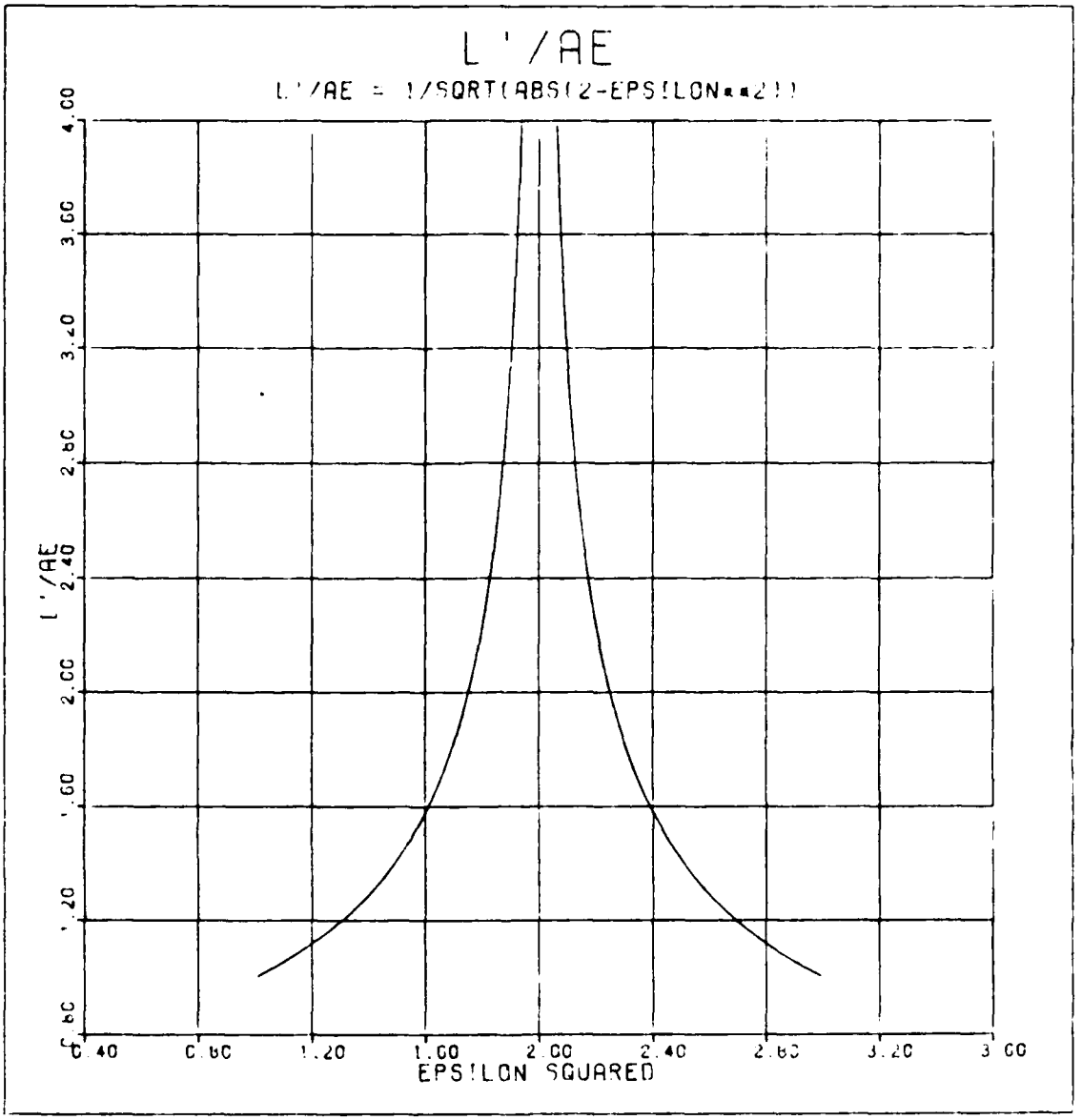

Figure 18 - Location of Primary Entrance Slit

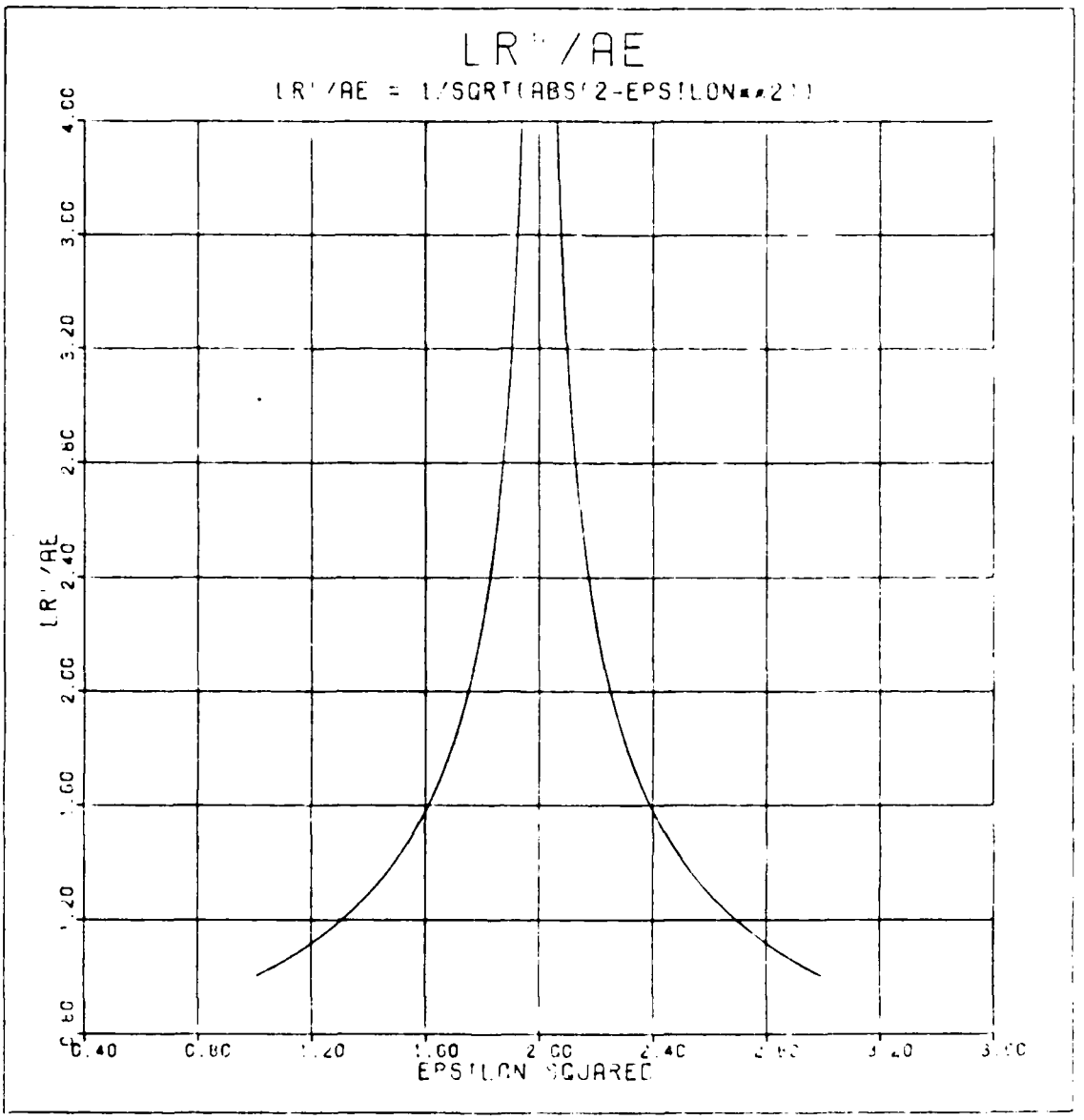

Figure 19 - Location of Radial Image Plane

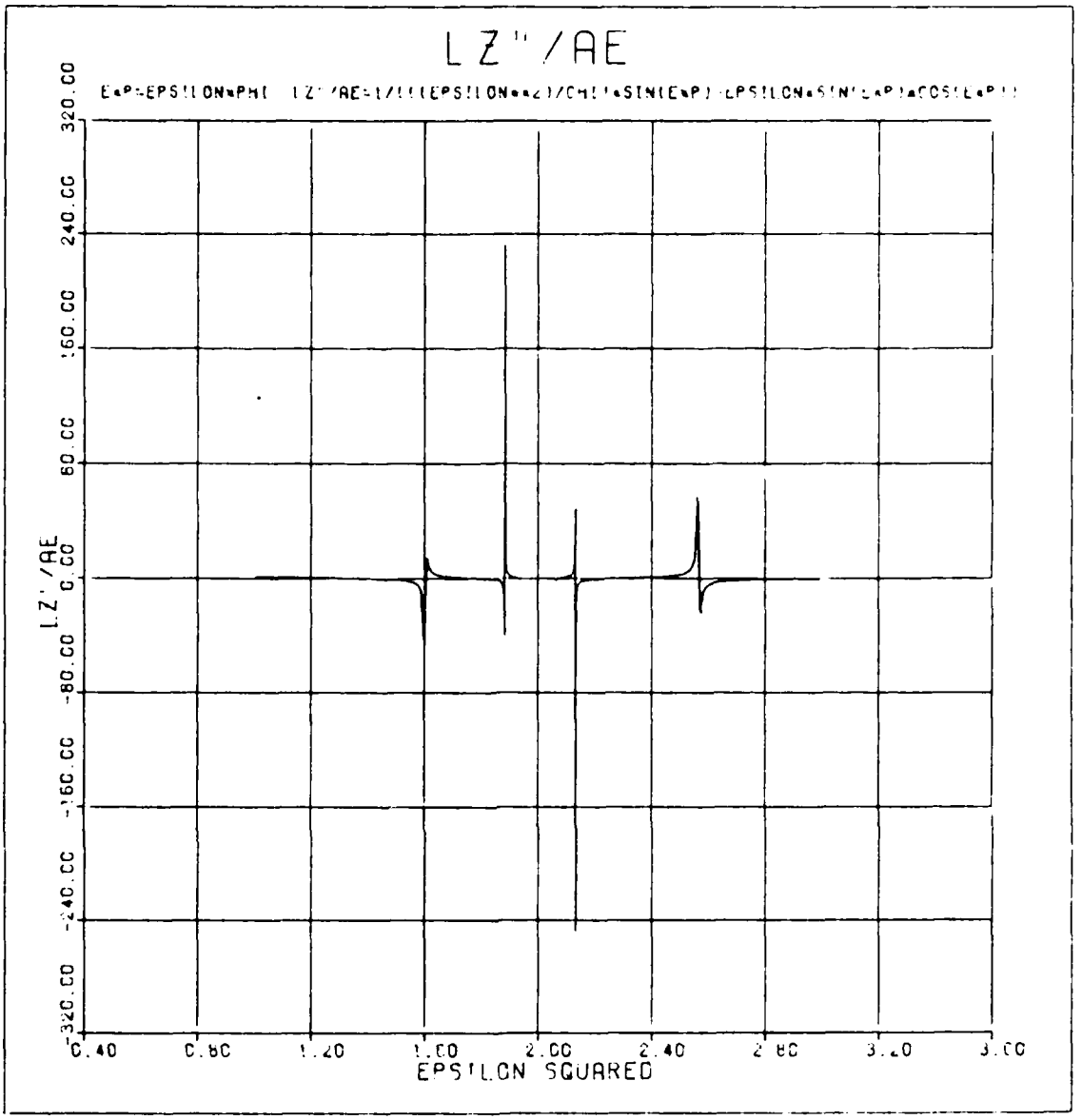

Figure 20 - Location of Axial Image Plane

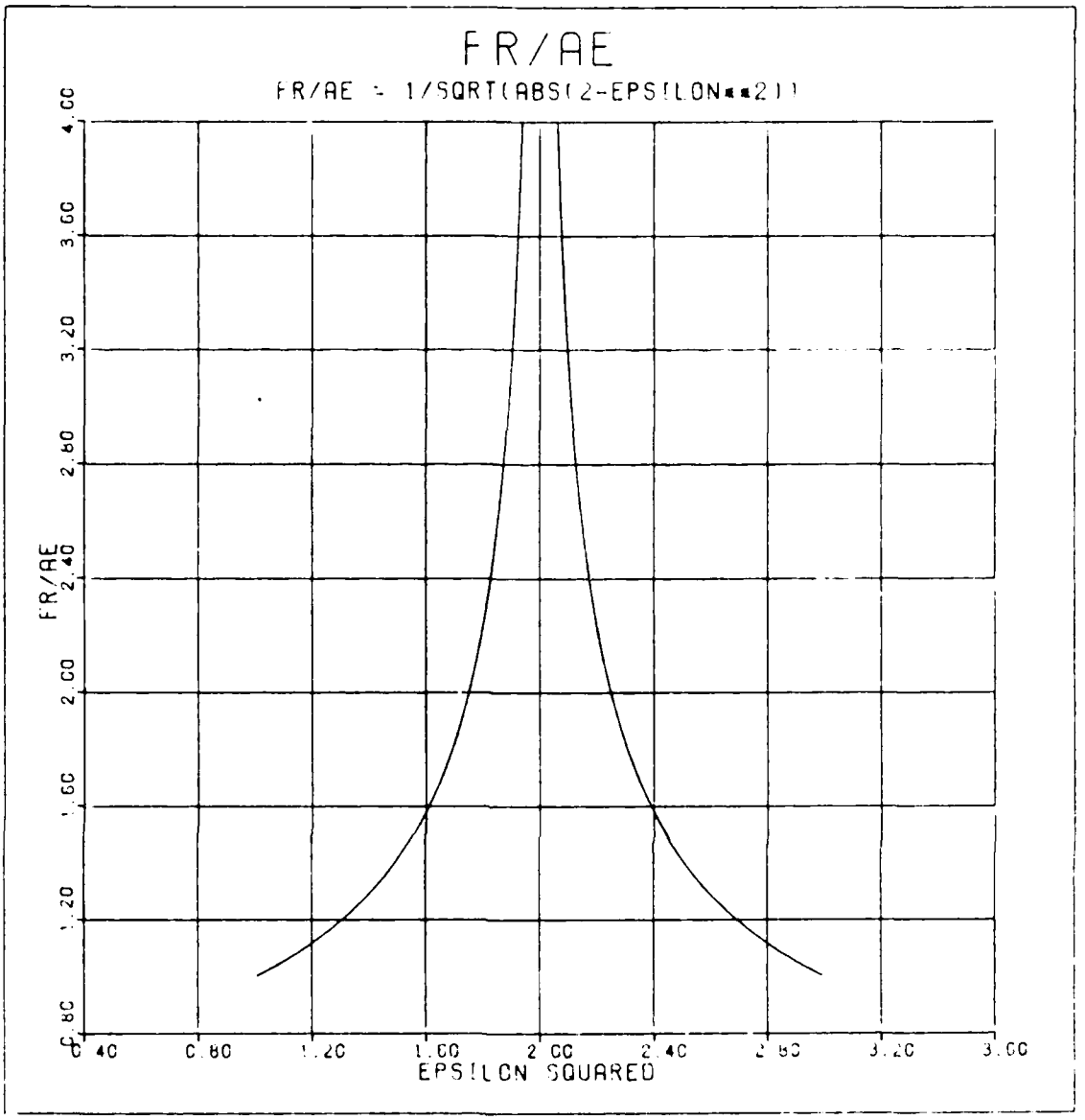

Figure 21 - Radial "Focal Length"

AD-A127 432 DESIGN STUDY OF A TOROIDAL ELECTROSTATIC ANALYZER(U) 2/2
AIR FORCE INST OF TECH WRIGHT-PATTERSON AFB OH SCHOOL
OF ENGINEERING R L HARTLEY DEC 82 AFIT/GEP/PH/82D-11
UNCLASSIFIED F/G 14/2 NL

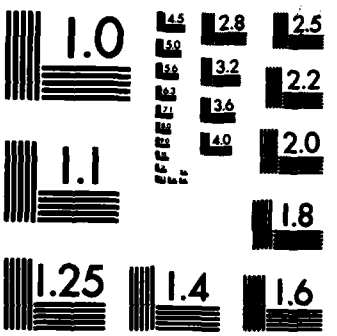

MICROCOPY RESOLUTION TEST CHART
NATIONAL BUREAU OF STANDARDS-1963-A

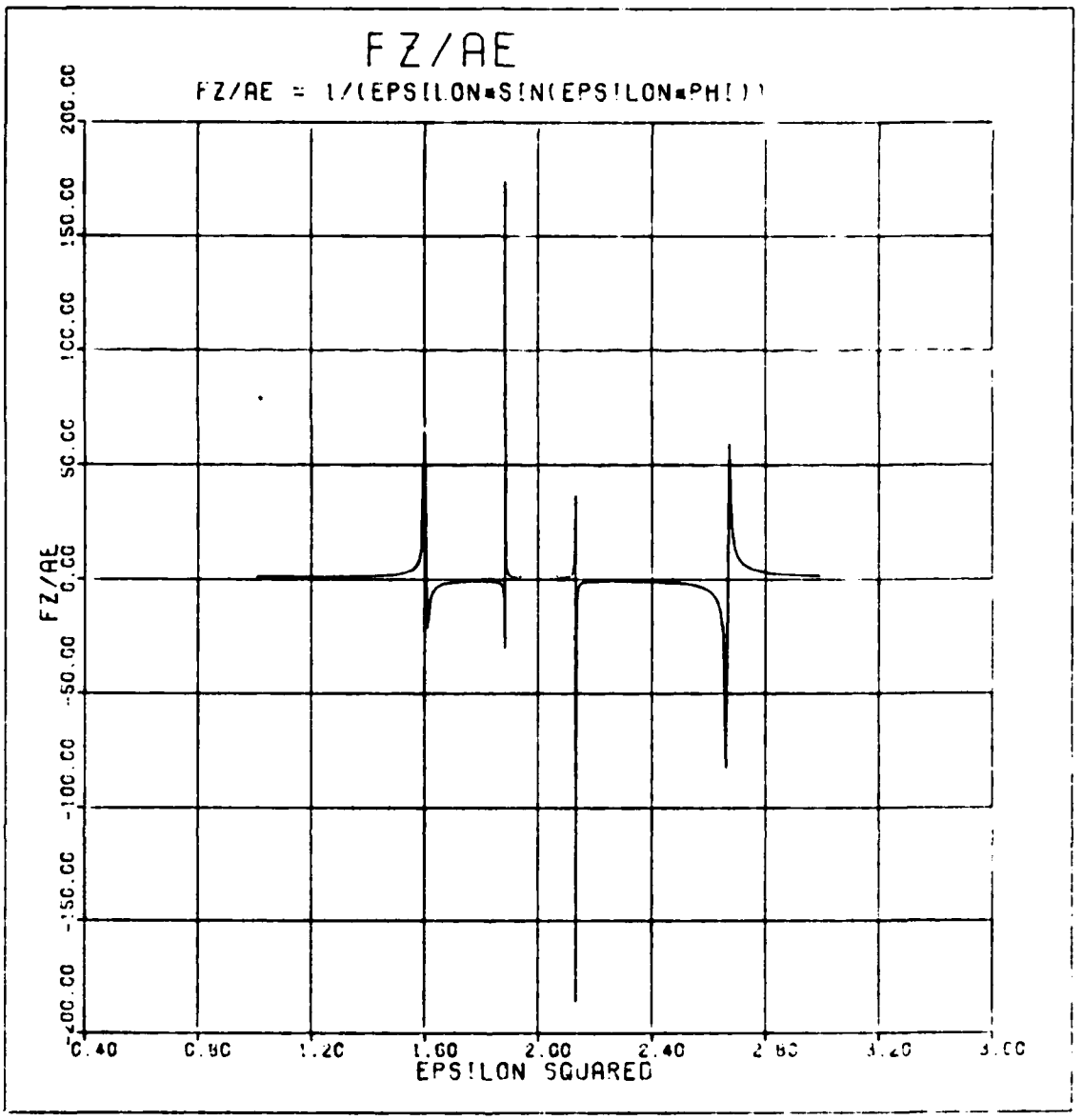

Figure 22 - Axial Focal Length

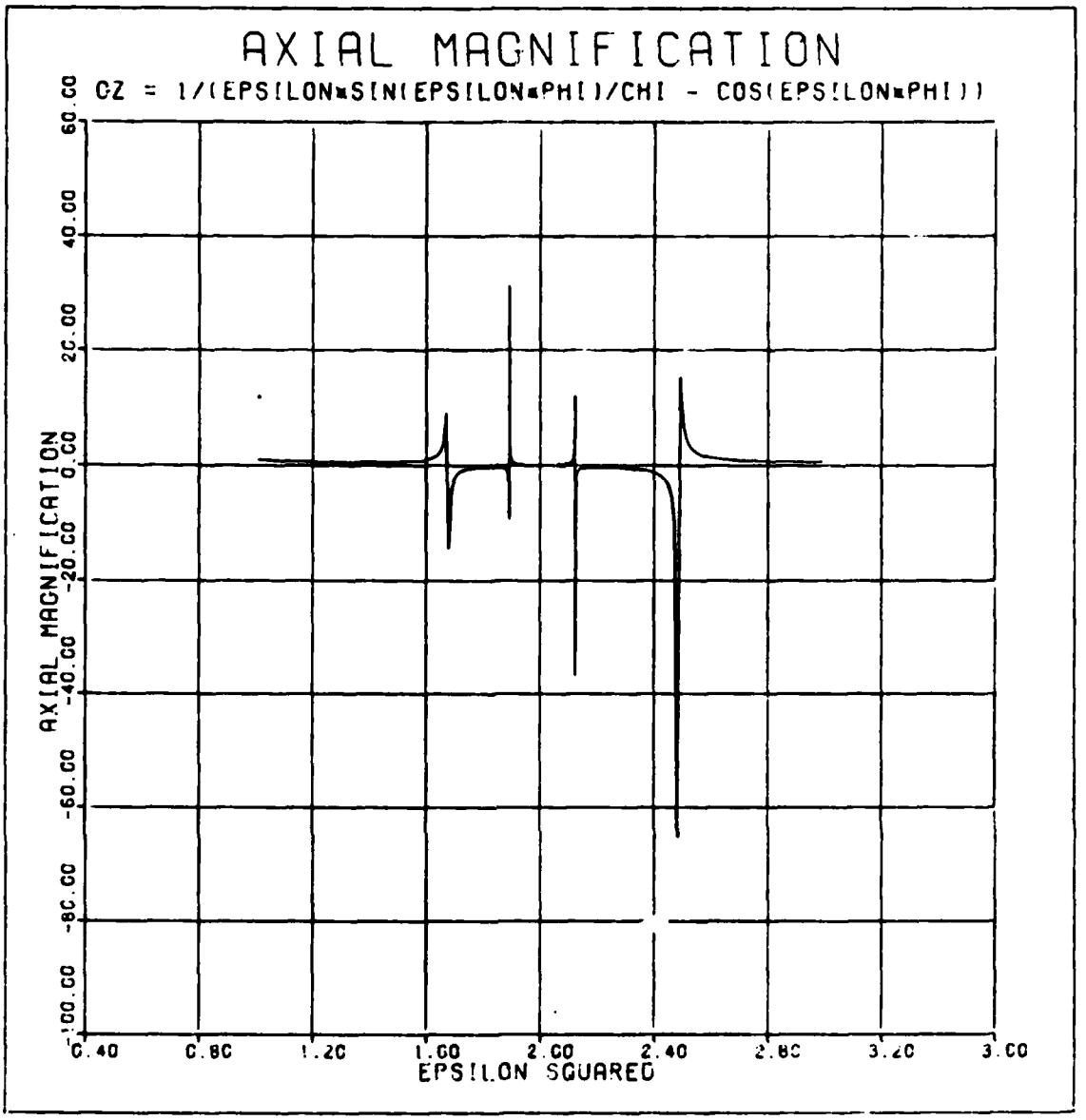

Figure 23 - Axial Magnification

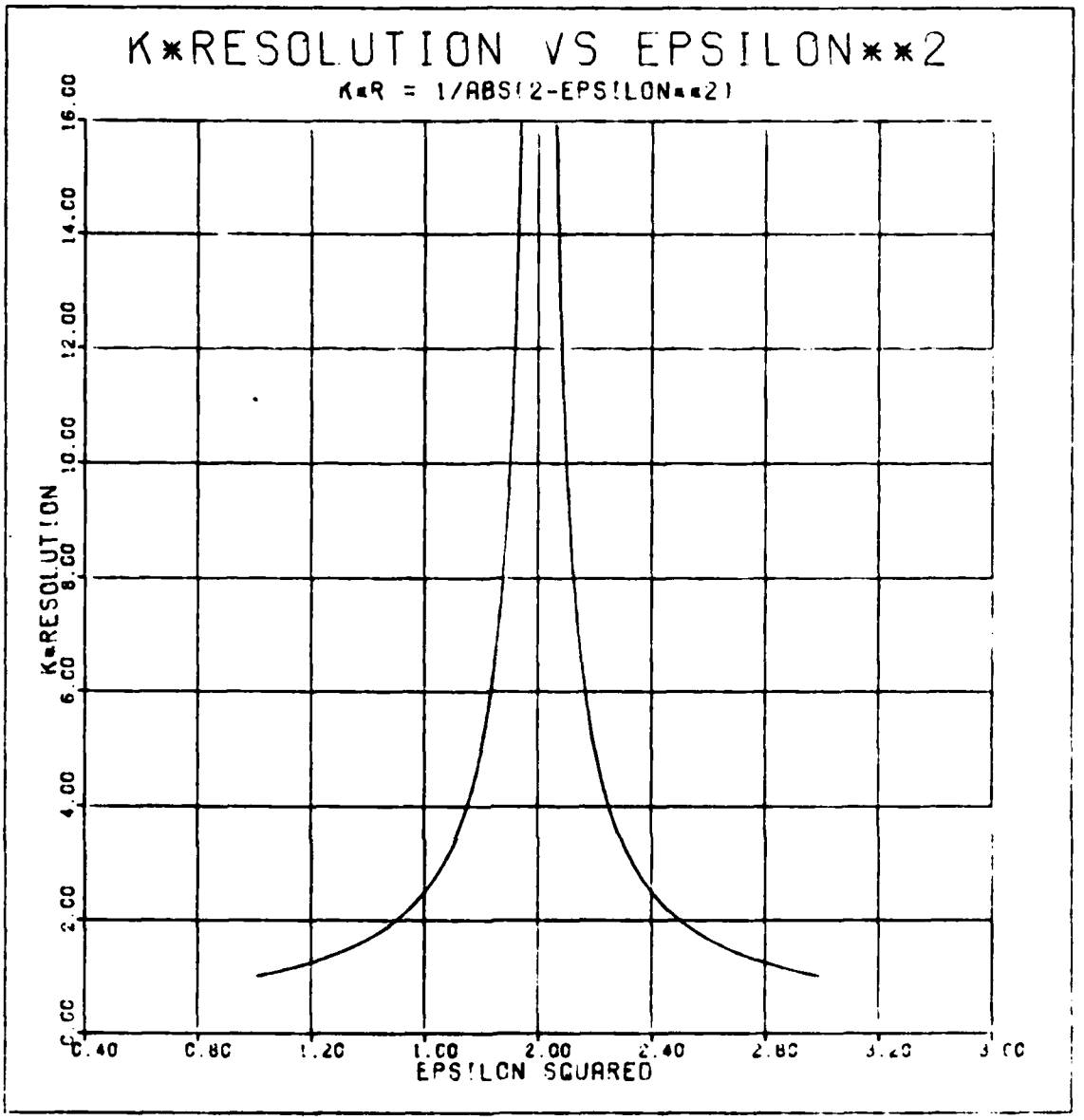

Figure 24 - Resolution

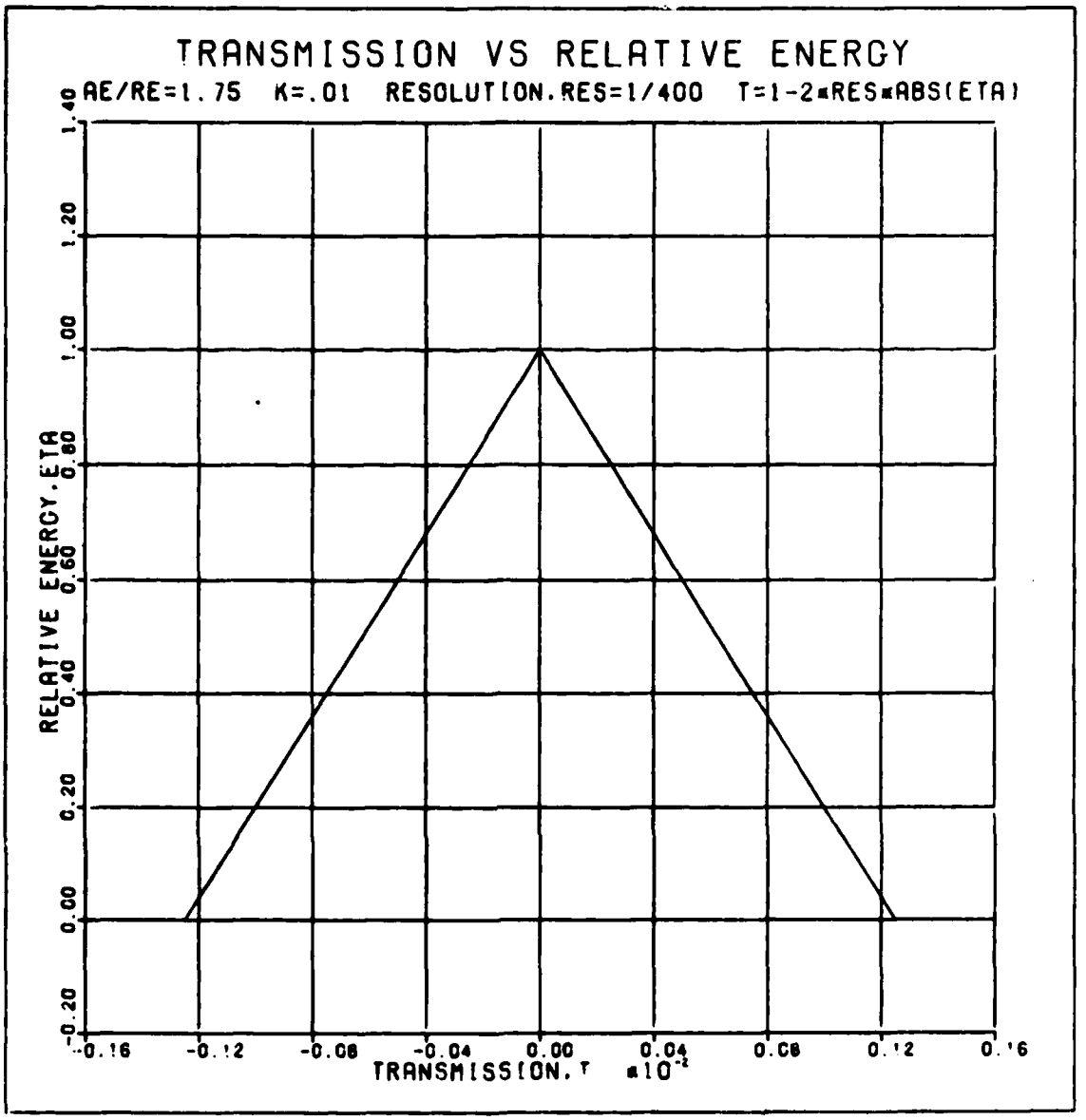

Figure 25 - Transmission

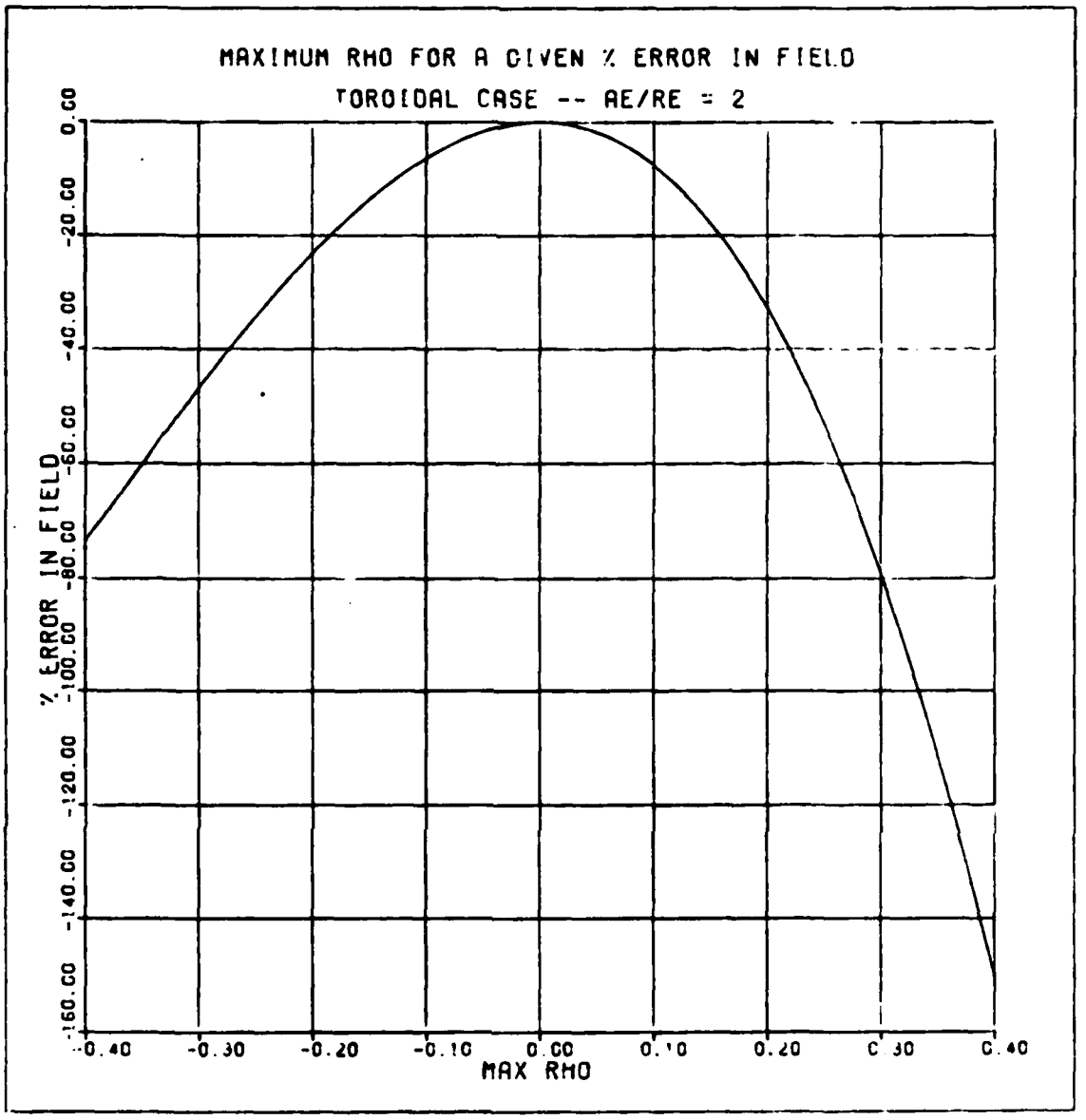

Figure 26 - % Error in Radial Electric Field

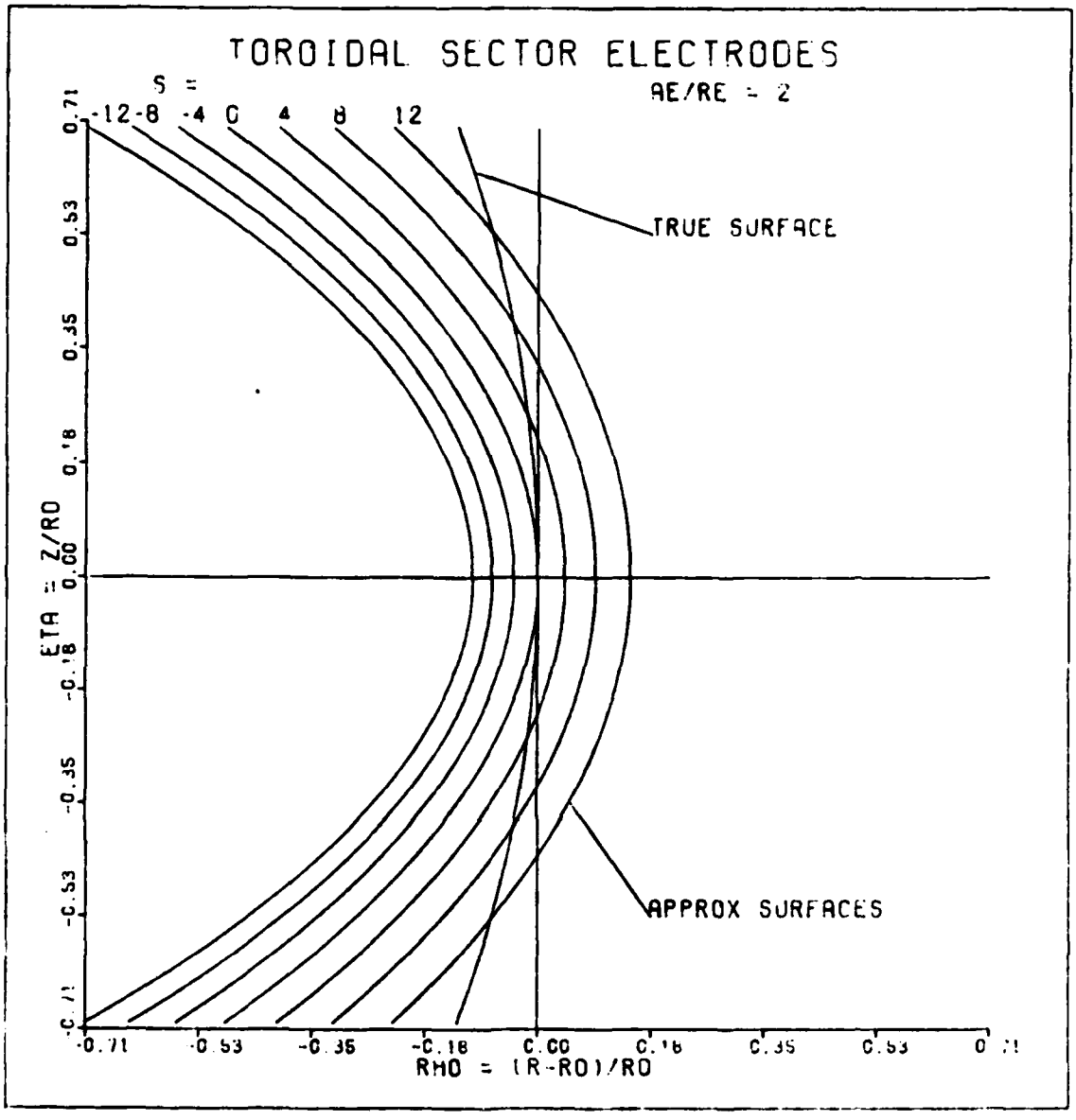

Figure 27 - Equipotential Curves

VITA

Robert LaVerne Hartley, Jr., was born on 24 April 1953 in Battle Creek, Michigan. He graduated from high school in Ft. Myers, Florida, in 1971. He attended the University of Miami and Edison Community College until he enlisted in the United States Navy in 1973. In 1974, he was transferred to the USAF-ROTC program at Florida State University, from which he received a Bachelor of Science degree in physics and a commission in the United States Air Force in 1978. He was then assigned to the Air Force Weapons Laboratory where he worked in the charged particle beam program until he entered the School of Engineering, Air Force Institute of Technology, in the Engineering Physics program, in June 1981.

Permanent Address: Box 4329 Rt 1, Jackfish Rd.
Bonita Springs, Florida 33923

UNCLASSIFIED

SECURITY CLASSIFICATION OF THIS PAGE (When Data Entered)

REPORT DOCUMENTATION PAGE	READ INSTRUCTIONS BEFORE COMPLETING FORM
1. REPORT NUMBER: AFIT/GEP/PH/82D-11	2. GOVT ACCESSION NO.: AD-A127432
	3. RECIPIENT'S CATALOG NUMBER
4. TITLE (and Subtitle): DESIGN STUDY OF A TOROIDAL ELECTROSTATIC ANALYZER	5. TYPE OF REPORT & PERIOD COVERED: MS Thesis
	6. PERFORMING ORG. REPORT NUMBER
7. AUTHOR(s): Robert L. Hartley, Jr. Capt USAF	8. CONTRACT OR GRANT NUMBER(s)
9. PERFORMING ORGANIZATION NAME AND ADDRESS: Air Force Institute of Technology (AFIT-EN) Wright-Patterson Air Force Base, Ohio 45433	10. PROGRAM ELEMENT, PROJECT, TASK AREA & WORK UNIT NUMBERS
11. CONTROLLING OFFICE NAME AND ADDRESS	12. REPORT DATE: December, 1982
	13. NUMBER OF PAGES: 92
14. MONITORING AGENCY NAME & ADDRESS(if different from Controlling Office)	15. SECURITY CLASS. (of this report): Unclassified
	15a. DECLASSIFICATION/DOWNGRADING SCHEDULE

16. DISTRIBUTION STATEMENT (of this Report)

Approved for public release; distribution unlimited

17. DISTRIBUTION STATEMENT (of the abstract entered in Block 20, if different from Report)

18. SUPPLEMENTARY NOTES

Approved for public release IAW AFR 190-17.
LYNN E. WOLAVER
Dean for Research and Professional Development
Air Force Institute of Technology (ATC)
Wright-Patterson AFB OH 45433
7 APR 1983

19. KEY WORDS (Continue on reverse side if necessary and identify by block number)

Electrostatic Analyzer
Electrostatic Prism
Toroidal
Ion Optics

20. ABSTRACT (Continue on reverse side if necessary and identify by block number)

The design of a toroidal, electrostatic analyzer is discussed with special emphasis on the instrument providing multiple channels of data by sampling different points of the energy spectra simultaneously. Two additional results of this study are that a toroidal analyzer can have four times the resolution of a spherical analyzer and can cover sixteen times as much of the energy spectra (with a fixed electrode voltage).

The electrostatics, equations of motion, and the optic equations are discussed. The applications chapter discusses the use of multiple, off-center

DD FORM 1 JAN 73 1473 EDITION OF 1 NOV 65 IS OBSOLETE

UNCLASSIFIED

SECURITY CLASSIFICATION OF THIS PAGE (When Data Entered)

slits, the minimization of the size of the instrument, the trade-offs that must be made in designing an instrument, the effect of field errors, the minimization of the effects of the field errors, and the total beam current as seen by the detector. Included in the appendix are design curves that should be of assistance to the reader in designing his own instrument.

END

FILMED

5-83

DTIC